PROF. ANDREW HURST (Orcid ID : 0000-0001-6775-3435)

Article type : Original Manuscript

**Mineralogical evidence for multiple dust sources in an early Triassic loessite**

**Wilson. M. J.,[2, 4] Hurst, A.,[1*] Wilkins, A. D.,[1] Wilson, L.[2] & Bowen. L.[3]**

[1]Department of Geology and Petroleum Geology, University of Aberdeen, Scotland, UK.[2]Environmental and Biochemical Sciences Group, James Hutton Institute, Aberdeen, Scotland, UK. [3]Department of Physics, Durham University, Durham, England, UK. [4]Tomsk Technical University, Tomsk, Siberia, Russia

[*]Corresponding author: email ahurst@abdn.ac.uk

**Associate Editor – Nick Lancaster**

**Short Title – Loessite with multiple ancient dust sources**

## ABSTRACT

Loessite present in a borehole into the Smith Bank Formation (early Triassic age, Central North Sea) differentiates five coeval source terranes for aerosol dust, three long distance sources and two local sources. All were active immediately following the end Permian mass extinction. Long distance sources are sedimentary, basic magmatic and acid–intermediate volcanic. Although predominantly silt-sized and dominated by quartz with subordinate feldspars, muscovite and illite, evidence of basic and acid–intermediate magmatic/volcanic sources are pervasive. Baddeleyite is diagnostic of basic magmatism, an origin supported by enrichment of plagioclase relative to potassium feldspar. Deduction of acid–intermediate

This article has been accepted for publication and undergone full peer review but has not been through the copyediting, typesetting, pagination and proofreading process, which may lead to differences between this version and the Version of Record. Please cite this article as doi: 10.1111/sed.12641

volcanism comes from the collective occurrence of irregular geometry quartz, volcanic shards, Ti-mineralization, euhedral biotite, sanidine, the co-occurrence of apatite and zircon, and the common occurrence of a tosuditic clay mineral. The tosuditic phase occurs as an unusual diagenetic dioctahedral chlorite/smectite formed at low temperature (<45°C), during very shallow burial by the decomposition of unstable rhyo-dacitic and andesitic grains in alkaline pore water from an adjacent lake that yielded pore fluids with a high Al:Si ratio. The Siberian Traps large igneous province is the likely source terrane for the magmatic and volcanic silt. Locally sourced clay pellets and kaolinite booklets formed from aeolian erosion of an adjacent, periodically desiccated lake-floor and a kaolinitic regolith, respectively. Inference of a prolonged harsh, arid climate leaves no evidence of any periods of sustained humidity or climatic fluctuation, such as pedogenesis. The association between the end Permian mass extinction, emplacement and aeolian erosion of the Siberian Traps large igneous province, and location of the Smith Bank Formation in a large lacustrine endorheic basin, combine to preserve a record of prolonged harsh climate in the early Triassic.

KEYWORDS. Aerosol dust, loessite, tosudite, volcanogenic input

## INTRODUCTION

Earlier work (Wilkins et al., 2017) made the first conclusive identification of loessite in a borehole section and derived diagnostic characteristics to differentiate it from associated fine-grained (silt-sized) lithologies. When viewed bedding parallel, randomly orientated granular texture, proved to be diagnostic of loessite, and was first characterized in the Smith Bank Formation (SBF) (Wilkins et al., 2017). The mineralogy of the SBF loessite from core in well 20/25-1 (UK) is unusual, possibly unique, and differentiates it from other similarly-aged, younger and older strata in the North Permian Basin of the North Sea (Wilkins et al., 2015; Wilkins, 2016; Wilkins et al., 2017). Clay mineralogy is particularly distinctive including significant quantities of a tosuditic clay mineral, dioctahedral regularly interstratified chlorite–smectite (Shimoda, 1978), which is unusual in sedimentary rock (Wilson, 2013), and kaolinite, which is unusual in the fine-grained strata in the Permo-Triassic of North Permian Basin of the Central North Sea (Ziegler, 2006). Worthy of note, is the occurrence of baddeleyite ($ZrO_2$), the first known occurrence of this mineral in sedimentary rock (Wilkins et al., 2015).

Mineralogy, and specifically clay mineralogy, is used to identify and characterize the source terrane of the aerosol dust that formed the loessite. Source terrane beyond the drainage basin catchment in which they deposited is congruent with modern-day aerosol dust, some of which transports thousands of kilometres from source (Nettleton & Chadwick, 1996; Mahowald et al., 2003; Koren et al., 2006). Such long-distance transport, largely following global wind circulation patterns, presents the opportunity for distinguishing multiple dust-sources operating simultaneously and ultimately combining to form loessite. During the early Triassic, the geological record north of 20ºN indicates a predominantly arid palaeo-climate with physical weathering prevailing (Roscher et al., 2011; Benton & Newell, 2013) and during which dust would be widely available.

A significant volcanic contribution to the SBF was suggested by Jeans (2006) and the present work looks for detailed evidence of volcanogenic mineralization along with a more exacting characterization of the unusual mineralogy documented earlier (Wilkins et al., 2015; Wilkins et al., 2017). Limited mineralogical characterization of loessite is previously reported with the exception of provenance studies using U/Pb dating of zircon (M. Soreghan et al., 2002; M. Soreghan et al., 2014), and very limited clay mineral analysis. Thus, little analogue data exist for this study. To counter the deficiency, the data herein are compared with studies on bentonite and tonstein that, although not aerosol dust *per se*, are air-fall deposits directly associated with volcanism.

## GEOLOGICAL SETTING

Deposition of the SBF in the North Permian Basin, records a period of Earth history that immediately followed the most severe known period of global mass extinction at the end Permian (Sahney & Benton, 2008). Emplacement of the Siberian Traps large igneous province (LIP) into coal and other carbonaceous sediments in Eastern Siberia, is inextricably associated with the extinction event (Wignall, 2005; Svensen et al., 2009; Jerram et al., 2016). The ensuing huge volume of carbon gases, including $CO_2$, and possible halocarbons released (Svensen et al., 2004; Retallack & Krull, 2006; Beerling et al., 2007; Payne & Kump, 2007) caused global climate change during a less than 2 Myr period of magmatism that extended over an area of 5 million $km^2$ (Reichow et al., 2009). Siberian LIP activity continued into the early Triassic (Reichow et al., 2009) and environmental stress and global warming similar to that experienced at the end Permian extended 4 to 5 Myr into the Triassic (Payne et al., 2004) during which deposition of the SBF occurred.

Although interpreted as a record of early Triassic recovery, the poor preservation of a very sparse fauna and flora confounds meaningful biostratigraphy (Goldsmith et al., 2003) and records pervasive aridity. Within this *ca* 5.8 Ma of very poorly constrained time the SBF loessite deposited and the core in well 20/25-1 represents at least 60 kyr of harsh arid climate (Wilkins et al., 2017). Location of borehole 20/25-1 is unusual on the western rift margin of the Central North Sea where the total Triassic interval is typically between 1500 m and less than 2000 m thick (Goldsmith et al., 2003, fig. 9.3). Later Mesozoic strata are absent or thin, and the area formed a stable platform high during the Upper Jurassic (Fraser et al., 2003) with <200 m of early Cretaceous calcareous mudstone-prone facies that thins westward.

In a local sedimentary and palaeo-environmental context, borehole 20/25-1 is located near the north-western margin of the large endorheic lake that occupied most of the North Permian Basin during the early Triassic (Goldsmith et al., 2003). There is no evidence of lacustrine processes in the 20/25-1 core, nor is there evidence for the activity of lake-marginal, ephemeral fluvial systems that fed the basin from the north-west (McKie & Williams, 2009). The physiographic isolation of the area adjacent to borehole 20/25-1 was a location where aerosol dust could accumulate with the only erosion and re-working restricted to minor autogenic pluvial episodes (Wilkins et al., 2017). Proving the presence of loessite defined an additional sedimentary facies to those summarized by Goldsmith et al. (2003) and led to several significant modifications to the early Triassic palaeo-environment in the North Permian Basin (Wilkins et al. 2017) that are entirely consistent with location in a subtropical climate zone (Roscher et al., 2011; Benton & Newell, 2013).

## MATERIALS

Samples were taken from continuous core from UK well 20/25-1 (Fig. 1A), located in Quad 20 in the UK sector of the Central North Sea (CBS), which was drilled to a depth of 1662 m (5453 ft). This well contains *ca* 11 m of loessite comprising predominantly unstratified siltstone with 0.6 m to 1.4 m bed thickness with occasional thin interlamination of stratified claystone, mudstone and siltstone that occur near the base and top of the cored interval (Wilkins et al., 2017). The interlaminae are compositionally similar to the unstratified strata and consist of reworked loessite. For exact locations of core samples, see Fig. 1B.

## METHODS

Optical microscopy characterized general mineralogy and fabric, X-ray powder diffraction (XRPD) quantified the mineralogy of both bulk grain samples and clay fractions. Scanning Electron Microscopy (SEM) with Energy Dispersive Spectroscopy (EDS) characterized the morphology and qualitative chemistry of the fine-grained phases present. Both bulk and clay (<2 µm) fractions were analysed by XRD, the results of the latter being used to identify and refine the analysis of the bulk material. Wilkins (2016) and Wilkins et al. (2017) describe the procedures in detail.

Scanning electron microscopy (SEM) used a Hitachi SU70 analytical high-resolution electron microscope (Hitachi Limited, Tokyo, Japan) equipped with an Oxford Instruments Aztec 3.3 energy-dispersive spectra (EDS; Oxford Instruments, Abingdon, UK) microanalysis system (G.J. Russell laboratory, Durham University). Two sample preparation methods were utilised. The first used a standard resin block with a diamond 1µm polishing finish. A Cressington 108 carbon-sputtering unit (Cressington Scientific Instruments, Watford, UK) provided a 25 nm carbon coating to all samples. Images were then obtained and investigated using 15Kev BSE (back-scattered electrons) for phase and chemical contrast imaging. The second sample preparation method involved careful cleaning of rock fragments that were then mounted using carbon cement followed by 30nm Au/Pd coating (Cressington 108Auto RF sputtering system). Secondary electron (SE) imaging at 8KeV was utilised for the purpose of depth of focus, topographical and natural state morphology of samples.

## RESULTS

### X-ray diffraction

Illite, chlorite, tosudite and kaolinite are present in the bulk samples (Table 1). Because tosudite is an unusual mineral in sedimentary rock (Wilson, 2013), it requires further comment. The first description of tosudite (Shimoda, 1969) emphasized its aluminous composition and dioctahedral structure. According to the definition of Bailey (1982), tosudite is only dioctahedral 'on average' and the chlorite component involved can be dioctahedral aluminous 2:1 layers with a hydroxide sheet of a trioctahedral brucitic ($Mg(OH)_2$) nature. A Mg-rich tosudite was described by Shimoda (1978). The mineral here termed tosudite (Table 2) is more appropriately described as a 'tosuditic clay' or a 'tosuditic phase' as the number of basal reflections indicating a completely regular chlorite–smectite structure is limited, and show only a tendency to regularity. However, its resistance to HCl treatment (Fig. 3) confirms its predominantly aluminous nature. For the sake of brevity, the term tosudite is used hereafter, but bearing in mind the caveat indicated above. The four clay minerals are persistent, irrespective of whether the strata are stratified or not, although tosudite is undetected in two samples. On average, the total percentage of clay minerals in the bulk rock is 35%, but varies from as little as 23% within a stratified mudstone (SB10), to as much as 41% within the loessite (SB05). Illite is the dominant clay mineral followed by tosudite > kaolinite > chlorite. However, detrital mica, mainly muscovite but also biotite, have the same (10Å) basal spacing as illite so the full pattern fit of the XRD trace does not effectively differentiate between them. Detrital mica and chlorite may therefore account for a portion of the clay fraction, possibly a large portion, of the values shown in Table 1. Samples with high dolomite cement have correspondingly low clay mineral content, a dilution effect caused by the pore-filling habit of dolomite.

The clay (<2 μm) fraction (Fig. 2 and Table 2) indicates the presence of the four clay minerals shown in Table 1 and in addition identifies the presence of a mixed-layer phase, which responds to ethylene glycol and is interpreted as ordered illite/smectite (I/S) with a high proportion of illite layers. This study notes that the relative proportions of clay minerals as assessed by analyses of bulk material and clay fractions are rather different, particularly with regard to the amount of illite and, the relative amounts of tosudite, kaolinite and chlorite. Illite forms a greater proportion of the bulk material than in the clay fraction, sometimes more than double, which confirms that there are significant amounts of micaceous material present in the non-clay fraction. Petrographic studies, which show the frequent presence of muscovite flakes up to 150 μm in length in siltstone samples, corroborate this. Kaolinite is approximately twice as abundant in the clay fraction as in the bulk material (compare Tables 1 and 2), from which one may infer that during extraction of the <2 μm fraction, disaggregation of large fragile kaolinite particles occurred. It follows that tosudite and chlorite, which show no significant increase in abundance between the bulk and clay fractions, do not have coarser grained progenitors prone to disaggregation.

Criteria by which illite, chlorite and kaolinite were identified are well-known and do not require repetition here, but this is not true of tosudite. In the air-dried state, tosudite has a peak at about 14Å with a broad shoulder developed at around 28Å (Fig. 3). These features represent the 002 and 001 basal reflections, respectively; higher order basal reflections are present. Ethylene glycol treatment causes expansion of both first and second order basal reflections to about 32Å and (more clearly) to 16Å, respectively, while heating at 300°C causes contraction of the 14Å peak to about 12Å. At this point, there is little difference in XRD characteristics between tosudite and corrensite, the most likely mineral to be confused with tosudite. However, tosudite is a dioctahedral Al-rich mineral (Shimoda, 1990), which is resistant to treatment with 6M HCl for 30 minutes at 95°C (the procedure of Hayashi & Oinuma, 1964), whereas corrensite, which is trioctahedral and Mg-rich, is not. It is clear that the present samples resist this treatment and are therefore dioctahedral and highly aluminous, a point confirmed by EDS analysis, which characterize tosudite.

**Thin section microscopy with back-scattered electron microscopy**

Unstratified loessite has a random fabric shown by the disposition of muscovite and biotite flakes (Fig. 4A). This appearance contrasts markedly with the stratified loessite in which a linear fabric is very clear, particularly where defined by the common orientation of muscovite flakes (Fig. 4B). Higher magnification images show clearly that both fabrics contain clay pellets or partly disaggregated clay pellets, which tend to be ellipsoidal (Fig. 4C). Some small areas of pore-filling pellets have similar appearance to the clay within pellets and are fragments of disaggregated pellets.

Subhedral to euhedral biotite-like mica has selectively foliated kaolinitisation (Fig. 4D) and exfoliated intercalation of kaolinite (Fig. 4E). Chlorite occurs in detrital lath-like grains or as laminar intercalations of micaceous particles (Fig. 4F). The chlorite has Mg-rich composition (Fig. 5A) and is associated with the chloritization of mica. There is no conclusive evidence that chlorite in the loessite formed diagenetically, although intercalation of chlorite between the exfoliated layers of mica could be interpreted as such. Quartz often has very irregular geometry with ragged margins, some of which is attributable to small quartz overgrowths (Fig. 6A). Jigsaw contacts occur between some grains (Fig. 6B) that are indicative of micro-fractures formed during mechanical compaction. Some micro-fractures in the largest quartz grains present have µm-scale inclusions, which sometimes form trails of fluid inclusions up to *ca* 2 µm across (Fig. 6A).

**Scanning electron microscopy of rock fragments**

The samples used for BSEM and petrographic analyses (Fig. 4) were sub-sampled for SEM examination (Wilkins et al., 2017). The SEM images of individual rock fragments show an essential similarity with regard to the morphology of clay minerals, and in many cases indicate unequivocal diagenetic origin. Widespread clay coatings cover and conceal detrital silt-size grains both in unstratified and stratified loessite.

Pore-filling clay in both stratified and unstratified facies has a pseudo-honeycomb appearance (Fig. 7A), a characteristic feature of smectitic clays when in a dried down state (Wilson, 2013, and references therein). In many instances, clay coatings are observed and EDS analysis reveals the co-occurrence of kaolinite and tosudite (Fig. 7B). All loessite samples have pervasive clay-coatings but locally have diagenetic minerals with euhedral crystal form. These include pyramidal crystals of quartz (Fig. 8A and B), rhombohedral dolomite (Fig. 8A) and kaolinite (Fig. 8C). Localization of euhedral quartz overgrowth reflects the availability of open pores into which quartz could grow, and the presence of quartz substrate below the clay coatings where quartz could nucleate. The association between diagenetic quartz and tosudite shows that quartz overgrowth post-dates tosudite genesis (Fig. 8B).

Kaolinite booklets (Fig. 8A) have platelet dimensions approximately five times larger than the irregularly packed vermicular kaolinite in which a large (>7 μm) micro-pore is present (Fig. 8C). A smooth clay coating is present on the vermicular kaolinite that may be the carapace of a clay pellet. There is no evidence that chlorite occurs in intersecting blade-like forms coating mineral grains (Welton, 1984) such as are commonly found in Permo-Triassic North Sea sandstone (Ziegler, 2006).

Other clearly diagenetic minerals include apatite, K-feldspar and albite. Apatite occurs as euhedral crystals, sometimes elongate in form, yielding strong Ca and P peaks (Fig. 9A and B). The feldspar minerals occur as small euhedral crystals showing a predominantly Al, Si composition containing Na (Fig. 9C and D) and K (Fig. 9A and B) for albite and K-feldspar, respectively. Euhedral cubic crystals of halite, yielding strong Na and Cl peals are observed (Fig. 9E and F), confirming their detection by XRPD. These are most likely diagenetic as the sample was from a fragment within the core rather than towards its edge.

## DISCUSSION

Located high on the rift margin of the Viking Graben, borehole 20/25-1 preserves a record of loessite sedimentation (Wilkins et al., 2017) followed by shallow burial relative to boreholes in the nearby Viking Graben. A maximum burial temperature of *ca* 45ºC, estimated from basin modelling (*supplementary data*), is significantly lower than the threshold for the onset of silicate and quartz diagenesis (*ca* 60°C, Nadeau, 2011). Preservation of minerals and textures related to aerosol deposition are thus likely, even with diagenetic mineralization, closely related to the original dust composition and unlikely related to thermally driven reactions during burial. Mineralogical data are fundamental to the understanding of the provenance of fine-grained strata, and mineralogy has precedence over geochemical data except when individual grains can be isolated in sufficient quantity, and are large enough, to allow micro-beam analysis (Hurst & Morton, 2014; Taylor & Macquaker, 2014). In silt and finer grade strata, such circumstances are unusual.

Mineralogical evidence exists for at least three long distance dust sources (*sensu* Yaalon, 1987), along with two local sources (Table 3). Quartz silt is the predominant mineral in the SBF loessite, and together with plagioclase, K-feldspar and muscovite form the bulk of the mineralogy (Table 1). This mineral assemblage is non-specific with respect to source terrane and assumed to record erosion of silt dust from weathered sedimentary strata, which were present over a large continental area to the north and north-east of the North Permian Basin (Fig. 13A). An exception to this is the anomalous enrichment of plagioclase feldspar relative to K-feldspar, the latter usually more common in Permo-Triassic northern European strata (Ali & Turner, 1982; Burley, 1984; Reeves et al., 2006). Of more terrane-specific value, are occurrences of baddeleyite (Wilkins et al., 2015) with associated plagioclase, and the relative abundance of several exotic grains/minerals and tosudite (Wilkins et al., 2017).

**Long distance dust provenance**

*Baddeleyite and plagioclase*

Discovery of scarce, tiny baddeleyite ($ZrO_2$) grains (Fig. 10A) from the Smith Bank Formation (SBF) loessite were the first ever record of this rare mineral in sedimentary rock (Wilkins et al., 2015). Typically, baddeleyite is associated with flood basalt terrane in large igneous provinces (LIPs) and its utility for U/Pb dating (Heaman & Le Cheminant, 1993). Mineral size and scarcity in the SBF preclude mineral separation obviating its utility for U/Pb radiometric dating (Brander et al., 2011). Given its rarity and limited range of parageneses (Heaman & Le Cheminant, 1993; Cabella et al., 1997), occurrence of baddeleyite is a strong diagnostic of provenance. Plagioclase feldspar is often associated with baddeleyite inclusions (Siivola, 1977; Scoates & Chamberlain, 1995), specifically associated with Si-poor basic magmatism (Heaman & Le Cheminant, 1993). Together the baddeleyite and anomalously high plagioclase content relative to K-feldspar (Table 1) support aerosol dust derivation from basic magmatic terrane (Fig. 12).

Two baddeleyite-bearing LIPs are candidate source terranes for the SBF loessite, the Neoproterozoic Volyn LIP and the late Permian to early Triassic Siberian Traps (Fig. 13A). In the early Triassic the Neoproterozoic Volyn LIP (Shumlyanskyy et al., 2016) was located *ca* 600 km ENE of the North Permian Basin. If exposed during the early Triassic, it is likely that lithification of the Volyn LIP made it an unlikely source of baddeleyite-bearing aerosol dust. By contrast, the Siberian Traps LIP is lithologically, temporally and spatially attractive as a source terrane. Magmatism and volcanism associated with its emplacement produced at least 2.5 x $10^6$ $km^2$ of flood basalt (Fedorenko et al., 1996). For *ca* 6 Ma (Reichow et al., 2009) prior to and during deposition of the SBF loessite, Siberian Traps flood basalts were exposed sub-aerially, subjected to weathering and erosion and located proximal to the track of Polar high pressure wind (Fig. 13A). Transport of aerosol is likely associated with this wind and the transport distance inferred for the baddeleyite-bearing dust is *ca* 4500 km. The Siberian Traps erupted huge volumes of $CH_4$ and $CO_2$ into the high atmosphere and made a major contribution to the end-Permian environmental crisis (Svensen et al., 2009; Jerram et al., 2016). An associated stream of aerosol dust would contribute to the harshness to the palaeo-climate.

*Volcanic dust and tosudite*

A collective body of evidence supports our contention that some of the loessite mineralogy is of volcanic origin and similar mineralogically to tonstein and bentonite. Presence of shards (Fig. 10B), although uncommon, is strong evidence of volcanic input (Fisher & Schmincke, 1984), and the associated Ti-mineralization is similar to that encountered in the non-marine sub-aqueous tuff deposits of tonstein (Spears, 2012). Reasons for Ti-enrichment of minerals in tonstein remain unexplained (Zhao et al., 2015; Hong et al, 2016). Quartz grains with highly irregular geometry (Figs 6 and 10B) are unlikely to form or preserve during sediment transport, being susceptible to breakage and abrasion. Inference of a more exotic provenance is the association with high-temperature or explosive volcanism, as preserved in tonstein of Permian (Dai et al., 2007) and Jurassic (Arbuzov et al., 2016) age. Neither of these analogues have comparable high-resolution data to this study.

Less diagnostic, but still significant is the occurrence of euhedral biotite, sanidine and, the co-occurrence of apatite and zircon. Large flakes of biotite are common in the SBF loessite, some with partial alteration to kaolinite (Fig. 4D and E). Biotite occurs in both bentonite and tonstein (Diessel, 1985; Huff & Morgan, 1990; Dai et al., 2007) and euhedral form in sedimentary strata is characteristic of volcanic origin (Spears, 2012). Generally, biotite is uncommon in sedimentary rock, specifically relative to muscovite. Sanidine is identified by XRD and by SEM, forming euhedral, tabular crystals of low symmetry with smooth pinacoid and prism faces and without etch marks. These observations are morphologically consistent with sanidine rather than orthoclase feldspar (Fig. 9A), although the observation is indicative rather than diagnostic. Apatite in the SBF loessite forms acicular, diagenetic crystals (Fig. 9A and B) and zircon is of detrital origin (Wilkins, 2016). In bentonite and tonstein the apatite + zircon assemblage is considered diagnostic of rhyolitic/dacitic origin (Spears, 2012). However, both minerals are common heavy minerals in sedimentary rock and, particularly in the case of ultra-stable zircon, have a wide range of paragenesis coupled with ultra-stability in physical and chemical weathering (Hurst & Morton, 2014). Apatite is notoriously susceptible to dissolution in weathering environments but frequently reappears during burial diagenesis (Morton, 2012), as observed in the SBF loessite.

Tosudite is unusual in sedimentary rock (Kulke, 1969; Wilson, 1971; Garvie, 1992; Hillier et al., 2006), mistakenly described as dioctahedral corrensite (Morrison & Parry, 1986; corrensite is trioctahedral), and typically abundant only in hydrothermally altered rock (Wilson, 2013, and references therein). Remarkably, in the SBF tosudite is volumetrically significant, an average of 6.7% of the bulk volume in the shallowest seven samples (Table 1), and up to 21% of the clay fraction (Table 2). If tosudite was detrital, it would require erosion of source terrane with a significant enrichment of tosudite being reworked into aerosol dust for a period of at least 60 kyr (Wilkins et al., 2017). Given the unusual occurrence of tosudite this is unlikely. Discussion of evidence for the diagenetic derivation of tosudite from precursor volcanic dust follows.

Although this study draws mineralogical comparison between the SBF loessite, bentonite and tonstein, they have important differences. Bentonite and tonstein form from geologically instantaneous deposits associated with volcanism (Haynes, 1994; Martin and Parris, 2007) whereas the aerosol dust that formed the SBF loessite accumulated gradually during a period of at least 60 kyr (Wilkins et al., 2017). Bentonite and tonstein form sub-aqueously whereas loessite forms sub-aerially; in the SBF loessite, sub-aerial deposition in an arid climate likely delayed the onset of diagenesis. Because loessite forms from a sub-aerial deposit, any volcanogenic grains present could not readily form smectite as in bentonite, which forms in subaqueous conditions (Grim & Güven, 1978; Moore & Reynolds, 1997). Evidence of pervasive oxidation characterizes the loessite and the present authors assume that it became water saturated only when fluctuations in the adjacent lake level to the southeast (Goldsmith et al., 2003) periodically caused inundation of groundwater into the loessite pore system. In loessite, the content of volcanic grains present is minor relative to grains derived from sedimentary source terrane whereas volcanic grains were the predominant (or sole) progenitors of bentonite and tonstein.  Despite loessite having a ‘dilute’ volcanic content, it shares mineralogical similarities with bentonite and tonstein, which support the presence of volcanic components. Quantification of the proportions of minerals from sedimentary, basic and acid to intermediate volcanic, terrane is not possible, mainly because most minerals have several possible origins (Fig. 11).

No known spatially proximal acid-intermediate volcanic source terrane occurs in the late Permian and early Triassic along the trajectory of the Polar high-pressure wind. However, the major and trace element geochemistry of claystone interbeds (tonstein) in coal from the Songzao Coalfield identify a probable contemporaneous rhyo-dacitic/andesitic volcanic terrane (Zhao et al, 2015). Perhaps of greater relevance to the SBF loessite are pyroclastic deposits associated with the Siberian traps LIP that occupy an area to the south of the basaltic flows (Jerram et al., 2016, fig. 1). These were a source of ejecta into the high atmosphere although their timing, composition and distribution are poorly understood (Kamo et al., 2006). If the volcanic ash contribution to the SBF loessite had a rhyo-dacitic/andesitic composition, its decomposition during early diagenesis may have formed diagenetic tosudite (Moore & Reynolds, 1997; Dai et al, 2014). Although acid-intermediate volcanism associated with the Siberian Traps is undocumented, occurrence of syenite in the Taymyr Peninsula records contemporaneous acid-intermediate magmatism. Associated silicic explosive eruptive centres are feasible but in LIPs these are typically poorly preserved and a specific origin for an acid-intermediate volcanic source terrane remains speculative. Record of non-basaltic components in redboles interbedded with Deccan floodbasalts are independent confirmation of acid–intermediate volcanism and airfall associated with LIP flood basalt (Ghosh et al. 2006; Schoene et al. 2019). A further possibility is that the SBF loessite records acid-volcanism not previously recognized in either the Siberian Traps, or elsewhere, along the aerosol route.

## Local dust provenance

*Silt-sized clay pellets*

Well-rounded, ellipsoidal clay pellets are common in the SBF loessite, 15% to >50% (Wilkins et al., 2017). The clay pellets are largely silt to very fine sand grade, are anomalously rounded relative to the angular framework grains, and form among the largest particles present (Fig. 4C and D) ranging from approximately 50 µm to >100 µm in length (coarse silt to approximately the very-fine to fine sand boundary). Location of the SBF loessite is windward of the prevailing south-east to north-west wind direction known from the southern margin of the North Permian Basin (Uličný, 2004), almost perpendicular to the Polar high pressure wind stream (Fig. 13A).

Morphologically similar pellets are important components of floodplains in both modern and ancient dryland fluvial systems in which they are associated with pedogenic processes (Rust & Nanson, 1989; Talbot et al., 1994; Wright & Marriot, 2007) or, from the clay dunes associated with saline lakes (Price, 1963; Bowler, 1973). Given the proximity to a major lacustrine system in which arid to hyper-arid climate prevailed (Goldsmith et al., 2003; Bourquin et al., 2011; Fig. 17A), pellets associated with clay dunes are more likely. There is little evidence of significant pedogenesis in the SBF loessite or the SBF in general (Wilkins, 2017). The balance of evidence supports the fact that persistent aeolian erosion of an adjacent exposed lake-floor that underwent periodic desiccation and efflorescence (cf. Bowler, 1973) is the source of the pellets (Wilkins et al., 2017). Laminar concentrations of clay pellets are present in the SBF loessite whereas they are absent elsewhere (Fig. 4). Modern clay dunes have similar lamination although quartzose grains in them are not associated with aerosol dust deposition (fig. 9, Bowler, 1973, and references therein). Lamination on a similar millimetre to centimetre scale (cf. Bowler, 1973) is not apparent in the SBF loessite.

*Kaolinite*

Kaolinite occurs as part of the clay mineral groundmass, as books and vermicules (Fig. 8A and C) and accounts for 10 to 20% of the clay mineral fraction (Table 2). Some kaolinite booklets are coarse silt size and larger than the framework grains and pores (Fig. 8A). Large size alone makes the kaolinite booklets unlikely diagenetic products in the loessite. Differences in kaolinite grain size and texture (Fig. 12) are strongly indicative of their different origins. Kaolinite with ragged booklet morphology are well known in kaolin and re-worked kaolin deposits (Keller, 1978) in which booklets become more ragged and finer-grained with reworking. Ragged kaolinite booklets similar in size to framework grains were associated with the reworking of a deeply weathered kaolinitic regolith (Bjørkum, et al., 1990). Occurrence of occasional coarse-silt kaolinite in the SBF loessite probably requires a source terrane other than an adjacent desiccated lake floor. Most likely is erosion of kaolinite-rich source terrane, which given the aridity of the Permo-Triassic in the study is likely to be pre-Permian.

A deeply weathered kaolinitised regolith of Upper Devonian age identified in northern Norway (Sturt et al., 1979), and similar kaolinitic deposits developed in Scotland (Monro et al., 1983) support the contention that widespread kaolinitic terrane was present prior to deposition of the SBF. Kaolins in southern Scandinavia (Gry, 1969; Norling, 1970), where they can be up to 60 m thick (Lidmar-Bergstrom, 1993), were inferred to be part of the same regolith that stretched over more than 14º latitude (Hurst, 1985). If correct, the southern Scandinavian kaolins are located along the trajectory of locally persistent, low-level wind from the south-east, and an attractive source of aeolian kaolinite to the windward of the North Permian Basin (Fig. 13B). Recent work on the southern Scandinavian kaolins (Lidmar-Bergström, 1993; Riber et al., 2015; Tan et al., 2016: Fredin et al., 2017) favours a Mesozoic (late Triassic to early Jurassic) age, which if correct excludes them as SBF source terrane.

Hydrothermally generated kaolin deposits are typically associated with granitoid intrusions (Wilson, 2013, and references therein), and less voluminous kaolin may form in vein deposits. Although not known as yet from the vast area of the Siberian Traps LIP (Svensen et al., 2009; Jerram et al., 2016) hydrothermal kaolinite would not be anomalous, and is spatially convenient to become incorporated in an aerosol dust stream. This is a much more speculative hypothesis than erosion of a kaolinitic regolith.

*Provenance summary*

Framework grains and illite comprise most of the SBF loessite, a mineralogy that is non-specific of a source terrane although probably largely reworked sedimentary rock. If the Polar high pressure (PHP) wind stream persisted and eroded the continental landmass north of the North Permian Basin it would be a significant conveyor of aerosol dust, some of which formed the SBF loessite (Fig. 13A). To deposit aerosol dust in the North Permian Basin, the trajectory of the PHP wind would on occasion need to deviate southward or, be deviated southward during interaction with the opposing Westerlies (Fig. 13). Long distance sourcing deposited minor quantities of unusual but diagnostic grains that form an assemblage associated with acid–intermediate volcanism and baddeleyite associated with basic magmatism (Fig. 11). Erosion of the Siberian Traps LIP, *ca* 4500 km to the north, is associated with baddeleyite. Combined with long distance sourcing, local sourcing derived clay pellets from the periodically desiccated adjacent lake and kaolinite silt from a source to the south-east (Fig. 13B).

## Diagenesis

During burial of the SBF loessite, low temperature (*supplementary data*) combined with a paucity of aqueous pore fluid for at least 60 kyr (Wilkins et al., 2017), removes two of the most significant drivers of diagenetic reactions in siliciclastic strata (Nadeau, 2011). A further difference of note in the SBF loessite is the absence of fine-grained organic matter, which is common in many fine-grained strata and often an associated as a factor in silicate diagenesis (Surdam et al., 1989). Prior to their discovery in the SBF loessite, the tosudite + kaolinite assemblage was unknown in sedimentary rock. At this low temperature, the assemblage of diagenetic minerals in siltstone is previously unrecorded although similar to assemblages developed in siltstone at higher temperature (Taylor & Macquaker, 2014). Clearly defined relationships between diagenetic minerals are visible only in large pores, thus definition of the sequence of diagenesis is challenging. Co-occurrence of diagenetic and detrital kaolinite further complicates these relationships.

### *Tosudite*

Determining the origin of tosudite is fundamental to understanding the relationship between the detrital composition of the loessite and diagenesis. Strong evidence for diagenetic origin is the pseudo-honeycomb texture (Figs 7A and 8B), which is virtually identical to that of diagenetic smectite in bentonite (Wilson, 2013). As a regularly interstratified chlorite/smectite mineral, tosudite may contain up to 50% smectitic layers, thus the honeycomb fabric is consistent with tosudite. Regular mixed-layer illite/smectite (identified by XRD) with a R3 stacking sequence and a low smectite content of between 8% and 21% (Moore & Reynolds, 1997) is, from a chemical perspective (EDS analysis), an alternative interpretation for the pseudo-honeycomb mineral. The R3 mixed-layer illite/smectite however, does not form a honeycomb texture (Keller et al., 1986). In the loessite, quartz overgrows tosudite (Fig. 8A and B) but tosudite coats kaolinite (Fig. 7B). Interestingly, the size (>10 μm across) of the kaolinite platelet coated by tosudite is similar to the irregular blocky kaolinite of detrital origin (Fig. 12) rather than a pre-tosudite diagenetic phase. Although tosudite with a pseudo-honeycomb texture is indiscernible in the matrix clay, this does not preclude a diagenetic origin for the matrix.

The high temperature required to synthesise tosudite (360°C, Matsuda & Henmi, 1983; 450°C, Ichikawa & Shimoda, 1976) and its natural occurrence in hydrothermal systems (Wilson, 2013, and references therein) are incompatible with the maximum burial temperature of *ca* 45°C estimated for the SBF loessite (*supplementary data*). Occurrence of volcanic grains (Fig. 11) combined with very limited pore fluid (from precipitation) and extreme oxidation (Bourquin et al., 2011; Wilkins et al., 2017), together with the *ca* 45°C thermal maximum, constrain tosudite paragenesis. Shallow subsurface ingress of lacustrine water during periods of lake-level fluctuation first introduced pervasive pore fluid to the loessite. Timing cannot be constrained but the prevailing aridity during the early Triassic in the North Permian Basin (Feist-Burkhardt et al., 2008; Roscher et al., 2011) and very slow rate of deposition (Wilkins et al., 2017) mean that it could occur immediately after the 60 kyr period of deposition or significantly later.

Tosudite is an aluminous clay mineral $(Na_{0.5}Al,Mg)_6[(Si,Al)_8O_{18}](OH)_{12} \cdot 5(H_2O))$ that to precipitate requires pore fluid with a high Al:Si ratio. Progenitor minerals for tosudite would initially be aluminous, and these are inferred here to be an aerosol dust of rhyo-dacitic/andesitic volcanic origin. Leaching during the ingress of alkaline lacustrine pore fluid from the adjacent lake (Bourquin et al., 2011), would decompose the glassy material present and tosudite formed. Preferential leaching of silica from the volcanic dust was sufficient to form diagenetic quartz, which is common in the SBF loessite and post-dates tosudite diagenesis (Fig. 8A and B). In this context, it is noteworthy that the detrital feldspar in the loessite has very limited evidence for etching, and thus is unlikely to contribute significantly to the formation of tosudite. Tosudite in SBF loessite is highly aluminous but also contains significant Mg (Fig. 7C), concentration of which is typically associated with trioctahedral structure. Tosudite is however, only dioctahedral 'on average' and can accommodate Mg elsewhere in its structure (Shimoda, 1978; Bailey, 1982). The limited data available on tosudite, and in particular from sedimentary rock, limits comparison between occurrences although significantly a volcanogenic association in sandstone is previously documented (Wilson, 1971; Garvie, 1992).

*Kaolinite*

Forming <5% of the bulk rock mineralogy (Table 1), some kaolinite occurs as part of the clay mineral groundmass as booklets and vermicules (Fig. 8A and C), which conventionally are indicative of diagenetic origin (Welton, 1984). In the loessite however, most of the coarse booklets and vermicules (Fig. 12A and B) are detrital. This interpretation is sustained by the combination of large size relative to pores and to other minerals present, possible inclusion within clay pellets (Fig. 8C), replacement by diagenetic quartz (Fig. 12A), textural similarity kaolinite reworked from weathering profiles (Keller, 1978; Bjørkum et al., 1990), and coating by diagenetic tosudite that otherwise appears to be the first formed diagenetic phase. In addition, the pervasively arid, oxidising environment during deposition and early burial is untypical for kaolinite formation (Singer, 1984; Hong et al., 2007). If the kaolinite is part of the same diagenetic paragenesis, it formed with no observed contemporaneous dissolution of plagioclase or potassium feldspar.

With the possible exception of apatite, other diagenetic minerals present are similar to those recorded from organic-rich siltstone (Taylor & Macquaker, 2014). Both K-feldspar and plagioclase feldspar (albite) occur as fine silt-sized (<10 μm), euhedral, tabular crystals without etch marks (Fig. 9A and B). Earlier discussion described the relationship between apatite and acid–intermediate volcanic provenance (Spears, 2012), and its possible diagenetic reappearance is consistent with that observed in sandstone diagenesis (Morton, 2012; Hurst & Morton, 2014).

**Loess and loessite**

Identification of loessite proved that large volumes of aeolian dust accumulated and preserved in ancient sedimentary basins (Johnson, 1989). Johnson (1989) speculated that loessite was likely present in similar northwest European basins, a speculation validated by Wilkins et al. (2017). No loessite (Soreghan, 1992; Chan, 1999; Soreghan et al., 2002, 2007; Wilkins et al., 2017) is associated with derivation of dust from glacial terrane, and the SBF loessite is the only one associated with a lacustrine environment (Wilkins et al., 2017). Independent of its provenance, latitude or altitude, loess is diverse in grain size, internal structure and mineralogy. Varying amounts of interbedding with coarser sediment, abundant evidence of alluvial and pluvial reworking, soil/palaeosol formation and generally regular variations in humidity are common (Gylesjö & Arnold, 2006; Iriondo & Kröhling, 2007; Stevens et al., 2013; Vandenberghe, 2013; Milodowski et al. 2015; Wang et al., 2015; Bird et al., 2015). By comparison, the SBF loessite is extremely homogenous with grain size variations only visible on a micro-scale, for example the presence of clay pellets, no evidence of palaeosols and centimetre-scale or less intervals of reworked loessite (Wilkins et al., 2017).

Clay mineralogical studies of loess focus mainly on identifying relationships between climate cyclicity and change, and clay mineral assemblages (Gylesjö & Arnold, 2006; Won et al., 2018). Largely these studies assume that detrital clay minerals record palaeoclimatic information from source terrane (Singer, 1984). Typical inferences are that kaolinite is generated during prolonged chemical weathering, Fe-rich chlorite disappears rapidly during chemical weathering, illite is a typical detrital component and that (pedogenic) smectite and illite/smectite are generated during moderate chemical weathering in poorly drained terrane, or in dry low latitudes. In loess sections from the Chinese Loess Plateau (CLP) there are statistically robust relationships between clay mineral assemblages and independent measures of climate variation (Won et al., 2018). This impressive study does not address how long-distance souring and local sourcing interact, nor does it consider the possible role of eroding clay mineral rich source terrane. Of course, these may not be significant issues on the CLP but they are demonstrably so in the SBF loessite.

The paucity of similar mineralogical data from other loessite, with the possible exception of Milodowski et al. (2015), compromises evaluation of whether the SBF loessite mineralogy is unusual or, for the time being, unique. Mineralogical studies of loess present similar comparative challenges, largely because clay mineral assemblages may be proxies for differentiation of climate change (Won et al., 2018). Monsoon-driven provenance changes identified in loessite (G. Soreghan et al., 2007; M. Soreghan et al., 2014) give a similar perspective, but using detrital zircon U/Pb dating. Similar detrital zircon U/Pb dating is applied to CLP loess provenance (Sun, 2002; Che & Li, 2013; Stevens et al., 2013; Sun et al., 2018). None of these studies resolves variation in mineralogy at the scale examined in the SBF loessite and all differ because they successfully identify evidence for significant climatic change.

So why is the SBF loessite so different? The unusual mineralogy of the SBF loessite is a consequence of several globally significant geological factors: deposition following the end Permian mass extinction, unusual mineralogy caused by long distance sourcing associated with the Siberian Traps LIP, insufficient rainfall to trigger significant pedogenesis, no evidence of significant erosion, and location on the leeward margin of a large endorheic lacustrine basin. Unlike any of the Cenozoic loess, deposition of the SBF loessite followed a global mass extinction. A major contributory factor to the mass extinction is the prolonged atmospheric pollution attributable to Siberian Traps LIP magmatic and volcanic activity (Wignall, 2005; Svensen et al., 2009; Jerram et al., 2016). Magmatic and volcanic activity continued into the early Triassic and contributed to the global slow recovery of biodiversity during and beyond the period of SBF deposition (Dickins, 1993; Meyer et al., 2011). Presence of baddeleytite and acid-intermediate volcanic dust progenitors to tosudite, together with other mineralogical factors (Fig. 11) link SBF loessite to Siberian Traps source terrane (Fig. 11). Similar mineralogical evidence is unknown in North American loessite of similar age; most North American loessite predates the end Permian mass extinction (Johnson, 1989; Soreghan, 1992; Evans & Read, 2007; Soreghan et al., 2007). Unlike Cenozoic CLP loess or other loessite, the SBF loessite has no evidence of prolonged periods of pedogenesis during which wet, intensified monsoonal conditions prevailed (M. Soreghan et al., 2014; Sun et al., 2016). It is reasonable to infer that the North Permian Basin received little direct rainfall in the *ca* 60 kyr preserved in the loessite, also a period during which it was exempt from significant monsoonal influence. Finally, the SBF loessite is distinctive by its location in an endorheic basin, adjacent to large alkaline lake (Goldsmith et al., 2003; Bourquin et al., 2011).

## CONCLUSIONS

The Smith Bank Formation (SBF) loessite preserves evidence of five terranes that sourced aerosol dust throughout most of a *ca* 60 kyr period in the early Triassic. Similar multiple dust sources in loessite or loess are previously unidentified. Sedimentary terrane was the predominant long-distance source, with evidence of subordinate basic volcanic/magmatic and acid to intermediate volcanic terranes, also representing long-distance sources. Clay pellets and reworking of a kaolinitic regolith constitute locally sourced dust.

Magmatism and volcanism associated with the emplacement of the Siberian Traps large igneous province (LIP) is the likely basic and acid–intermediate magmatic source terrane, approximately 4500 km distant from the SBF loessite. Baddeleyite ($ZrO_2$), only twice identified in sedimentary rock, is diagnostic of basic volcanic/magmatic terrane, along with enrichment of plagioclase relative to K-feldspar. Grains indicative of acid to intermediate volcanic terrane include irregular geometry quartz, volcanic shards, Ti-mineralization, euhedral biotite, sanidine, the co-occurrence of apatite and zircon, and occurrence of tosudite. Aerosol dust was carried south and south-east by Polar high-pressure wind, and is the first record of ancient global aerosol dust transportation and first direct evidence volcanic detritus in the Triassic of the North Sea.

Local aeolian sourcing of pervasive clay pellets and ragged kaolinite booklets from the south-east adds complexity to the mineralogy and texture of the loessite. Clay pellets derived from erosion of an adjacent periodically dry lake floor are the coarsest grains present and are locally concentrated. Erosion of kaolinitised regolith, probably exposed to the immediate south-east of the North Permian Basin, is the inferred source terrane for the ragged kaolinite booklets. The authors are unaware of previous records of similar clasts in loessite.

Tosudite is volumetrically significant in the loessite and associated with low temperature (< *ca* 45°C), shallow burial decomposition of acid-intermediate volcanic aerosol dust when inundated by alkaline, lacustrine pore water. Low temperature formation of tosudite is previously unrecorded but has a similar paragenetic environment to tonstein and bentonite mineralization. Occurrence of tosudite, and some earlier work where it has been misidentified, lead to the suggestion herein that it may be more common in sedimentary strata than is hitherto assumed.

Comparison with other loessite and loess shows that the SBF loessite lacks evidence of pedogenesis or other indicators of possible climatic fluctuation; only faint possible traces of life are present in the SBF loessite (Wilkins et al., 2017). In contrast, it records sustained aridity and oxidation caused by the association between the emplacement and aeolian erosion of the Siberian Traps LIP, the Polar high-pressure wind dust-conveyor and location of the SBF in a large lacustrine endorheic basin.

**ACKNOWLEDGEMENTS**

ADW acknowledges with thanks Steve Hillier of the James Hutton Institute for guiding her through the procedures of the X-ray identification of clay minerals and quantitative mineralogical analysis. MJW is appreciative for the SEM examination of various rock fragments by Evelyne Delbos, also of the James Hutton Institute. Simon Kemp, Nick Lancaster and Nigel Mountney provided insightful review and editorial comments for which we are hugely grateful.

## REFERENCES


**Ali, A.D.** and **Turner, P.** (1982) Authigenic K-feldspar in the Bromsgrove sandstone formation (Triassic) of central England. *Journal of Sedimentary Research, 52, 187-197.*

**Arbuzov, S. I., Mezhibor, A. M., Spears, D. A., Ilenok, S. S., Shaldybin, M. V.** and **Belaya, E. V.** (2016) Nature of tonsteins in the Azeisk deposit of the Irkutsk Coal Basin (Siberia, Russia). *International Journal of Coal Geology*, **153**, 99-111.

**Bailey, S. W.** (1982) Nomenclature for regular interstratifications. *American Mineralogist,* **67**, 394-398.

**Beerling, D.J., Harfoot, M., Lomax, B.** and **Pyle, J.A.** (2007) The stability of the stratospheric ozone layer during the end-Permain eruption of the Siberian Traps. *Philos. Trans. Royal Soc., Math. Phys. Eng. Sci*., **365**, 1843–1866.

**Benton, M.J.** and **Newell, A.J.** (2013) Impacts of global warming on Permo-Triassic terrestrial ecosystems. *Gondwana Res*., **25**, 1308–1337.

**Bird, A., Stevens, T., Rittner, M., Vermeesch, P., Carter, A., Andò, D., Garzanti, E., Lu, H., Nie, J., Zhang, H.** and **Xu, Z.** (2015) Quaternary dust source variation across the Chinese Loess Plateau. *Palaeogeography, Palaeoclimatology, Palaeoecology*, **435**, 254-264.

**Bjørkum, P.A., Mjøs, R., Walderhaug, O.** and **Hurst, A.** (1990) The role of the late Cimmerian unconformity for the distribution of kaolinite in the Gullfaks Field, northern North Sea. *Sedimentology*, **37**, 395-406.

**Bourquin, S, Bercovici, A., López-Gómez, J., Diez, J. B., Broutin, J., Ronchi, A., Durand, M., Arché, A., Linol B.** and **Amour, F.** (2011) The Permian–Triassic transition and the onset of Mesozoic sedimentation at the northwestern peri Tethyan domain scale: Palaeogeographic maps and geodynamic implications. *Palaeogeography, Palaeoclimatology, Palaeoecology*, **299**, 265–280.

**Bowler, J.M.** (1973) Clay dunes: their occurrence, formation and environmental significance. *Earth-Sci. Rev.*, **9**, 315– 338.

**Brander, L., Söderlund, U.** and **Bingen, B.** (2011) Tracing the 1271–1246 Ma Central Scandinavian Dolerite Group mafic magmatism in Fennoscandia: U–Pb baddeleyite and Hf isotope data on the Moslätt and Børgefjell dolerites. *Geological Magazine*, **148**, 632–643.

**Burley, S.** (1984) Patterns of diagenesis in the Sherwood Sandstone Group (Triassic), United Kingdom. *Clay Minerals*, *19*, 403-440.

**Cabella, R., Gazzotti, M.** and **Lucchetti, G.** (1997) Loveringite and baddeleyite in layers of chromium spinel from the Bracco Opiolitic Unit, northern Appenines, Italy. *Canadian Mineralogist*, **35**, 899-908.

**Chan, M. A.** (1999) Triassic loessite of north-central Utah; stratigraphy, petrophysical character, and paleoclimate implications. *Journal of Sedimentary Research*, **69**, 477-485.

**Che, X.** and **Li, G.** (2013) Binary sources of loess on the Chinese Loess Plateau revealed by U-Pb ages of zircon. *Quaternary Research*, **80**, 545-551.

**Dai, S., Li, T., Seredin, V.V., Ward, C.R., Hower, J.C., Zhou, Y., Zhang, M., Song, X., Song, W.** and **Zhao, C.** (2014) Origin of minerals and elements in the Late Permian coals, tonsteins and host rocks of the Xinde Mine, Xianwei, eastern Yunnan, China. *International Journal of Coal Geology,* **121**, 53-78.

**Dai, S.F., Zhou, Y.P., Ren, D.Y., Wang, X.B., Li, D.** and **Zhao, L.** (2007) Geochemistry and mineralogy of the Late Permian coals from the Songzao Coalfield, Chongqing, southwestern China. *Science in China Series D: Earth Sciences,* **50**, 678-688.

**Dickins, J.M.** (1993) Climate of the Late Devonian to Triassic. *Palaeogeography, Palaeoclimatology, Palaeoecology,* **100**, 89-94.

**Diessel, C.F.K.** (1985) Tuffs and tonsteins in the Coal Measures of New South Wales, Australia. *10th Congres International de Stratigraphie et de Geologie du Carbonifere, Madrid*, **4**, 197–210.

**Evans. J.E. and Reed, J.M.** (2007) Integrated loessite-paleokarst depositional system, early Pennsylvanian Molas Formation, Paradox Basin, southwestern Colorado, U.S.A. *Sedimentary Geology*, **195**, 162-181.

**Fedorenko, V.A., Lightfoot, P.C., Naldrett, A.J., Czamanske, G.K., Hawkesworth, C.J., Wooden, J.L.** and **Ebel, D.S.** (1996) Petrogenesis of the flood-basalt sequence at Noril'sk, North Central Siberia. *Int. Geol. Rev.,* **38**, 99–135.

**Feist-Burkhardt, S., Götz, A. E., Szulc, J., Borkhataria, R., Geluk, M., Haas, J., Hornung, J., Jordan, P., Kempf, O., Michalik, J., Nawrocki, J., Reinhardt, L., Richen, W., Rholing, H.-G., Rűffer, T., Török, Á** and **Zühlke, R.** (2008) Triassic. *In*: McCann, T. (ed) *The Geology of Central Europe, Volume 2: Mesozoic and Cenozoic,* The Geological Society, London, pp. 749-822.

**Fisher, R.V.** and **Schmincke, H-U.** (1984) *Pyroclastic rocks*. Springer-Verlag Berlin Heidelberg, p. 472.

**Fraser, S., Robinson, A., Johnson, H., Underhill, J. Kadolsky, D., Connell R.** and **Ravnås, R.** (2003) Upper Jurassic. *In:* Evans, D., Graham, C., Armour, A. & Bathurst, P. (eds) *The Millenium Atlas: Petroleum Geology of the Central and Northern North Sea*. The Geological Society, London, 157–189.

**Fredin, O., Viola, G., Zwingmann, H., Sørlie, R., Brönner, M., Lie, J-E., Grandal, E.M., Müller, A., Margreth, A., Vogt, C.** and **Knies, J**. (2017) The inheritance of a Mesozoic landscape in western Scandinavia. *Nature Communications,* **8**, 14879, DOI: 10 .1038 /ncomms14879.

**Garvie, L.A.J.** (1992) Diagenetic tosudite from the lowermost St Maughan's Group, Lydney harbour, Forest of Dean, UK. *Clay Minerals,* **27**, 507-503.

**Gosh, P., Sayeed, M.R.G., Islam, R. and Hundekari, S.M.** (2006) Inter-basaltic clay (bole bed) horizons from Deccan traps of India: Implications for palaeo-weathering and palaeo-climate during Deccan volcanism. *Palaeogeography Palaeoclimatology Palaeoecology*, **242**, 90–109.

**Goldsmith, P.J., Hudson, G.** and **van Veen, P.** (2003) Triassic. *In:* Evans, D., Graham, C., Armour, A. & Bathurst, P. (eds) *The Millenium Atlas: Petroleum Geology of the Central and Northern North Sea*. The Geological Society, London, 105–127.

**Goldsmith, P.J., Rich, B.** and **Standring, J.** (1995) Triassic stratigraphy in the South Central Graben, UK North Sea. *In:* Boldy, S.A.R. (ed.) *Permian and Triassic Rifting in Northwest Europe*. The Geological Society, London, Special Publication, **91**, 123–143.

**Grim, R.** and **Güven, N.** (1978) Bentonites: Geology, Mineralogy, Properties and Uses. Developments in Sedimentology v. **24**, Elsevier, 256 p.

**Gry, H., Jøgart, T.** and **Poulsen, V.** (1969) Geologi pa Bornholm *Varv Ekeskursjonsfmernx*. **1**, Kobenhavn, 47-51.

**Gylesjö, S,** and **Arnold, E.** (2006) Clay mineralogy of a red clay-loess sequence from Lingtai, the Chinese Loess Plateau. *Global and Planetary Change*, **51**, 181-194.

**Hayahsi, H.** and **Oinuma, K.** (1964) Behaviours of clay minerals in treatment with hydrochloric acid, formamide and hydrogen peroxide. *Clay Science*, **2**, 75-91.

**Haynes, J.T.** (1994) The Ordovician Deicke and Millbrig K-Bentonite Beds of the Cincinnati Arch and the Southern Valley and Ridge Province. *Geological Society of America, GSA Special Paper*, 290, doi.org/10.1130/SPE290.

**Heaman, L.M.** and **LeCheminant, A.N.** (1993) Paragenesis and U-Pb systematics of baddeleyite (ZrO2). *Chemical Geology,* **110,** 95-126.

**Hillier, S., Wilson, M. J.** and **Merriman, R. J.** (2006) Clay mineralogy of the Old Red Sandstone and Devonian sedimentary rocks of Wales, Scotland and England. *Clay Minerals,* **41**, 433-471.

**Hong, H. L., Li, Z, Xue, H. J., Zhu, Y. H., Zhang, K. X.,** and **Xiang, S. Y.** (2007) Oligocene clay mineralogy of the Linxia basin: evidence of palaeoclimatic evolution subsequent to the initial-stage uplift of the Tibetan plateau. *Clays and Clay Minerals*, **55**, 491–505.

**Hong, H., Fang, Q., Lulu Zhao, L., Schoepfer, S., Wang, C., Gong, N., Li, Z. and Chen, Z-Q.** (2016) Weathering and alteration of volcanic ashes in various depositional settings during the Permian-Triassic transition in South China: mineralogical, elemental and isotopic approaches. *Palaeogeography, Palaeoclimatology, Palaeoecology*, http://dx.doi.org/10.1016/j.palaeo.***2016***.06.026.

**Huff, W.D.** and **Morgan, D.J.** (1990) Stratigraphy, mineralogy and tectonic setting of Silurian K-bentonites in Southern England and Wales. In: Farmer, V.C., Tardy, Y. (eds.), *Proceedings, 9th International Clay Conference, Strasbourg 1989*: Sci. Geol. Mem., **88**, 33–42.

**Hurst, A.** (1985) The implications of clay mineralogy to palaeoclimate and provenance during the Jurassic in NE Scotland. *Scottish Journal of Geology*, **21**, 143-160.

**Hurst, A.** and **Morton, A.C.** (2014) Provenance models: the role of sandstone mineral-chemical stratigraphy. In: *Sediment Provenance Studies in Hydrocarbon Exploration and Production*, Scott, R.A., Smyth, H.R., Morton, A.C. and Richardson, N. (eds). Geological Society of London, Special Publication, **386**, 7-26.

**Ichikawa, A.** and **Shimoda, S.** (1976) Tosudite from the Hokuno mine, Hokuno, Gifu Prefecture, Japan. *Clays Clay Minerals,* **24**, 142-148.

**Iriondo, M.H.** and **Kröhling, D.M.** (2007) Non-classical types of loess. *Sedimentary Geology*, **202**, 352-368.

**Jeans, C.V.** (2006) Clay mineralogy of the Permo-Triassic strata of the British Isles: onshore and offshore. *Clay Minerals*, **41**, 309-354.

**Jerram, D.A., Svensen, H.H., Planke, S., Polozov, A.G.** and **Torsvik, T.H.** (2016) The onset of flood volcanism in the north-western part of the Siberian Traps: explosive volcanism versus effusive lava flows. *Palaeogeography Palaeoclimatology Palaeoecology*, **441**, 38-50.

**Johnson, S.Y.** (1989) Significance of loessite in the Maroon Formation (middle Pennsylvanian to lower Permian), Eagle Basin, Northwest Colorado. *J. Sed. Petrol.*, **59**, 782–791.

**Kamo, S.L., Crowley, J.** and **Bowring, S.A.** (2006) The Permian–Triassic boundary event and eruption of the Siberian flood basalts: an inter-laboratory U–Pb dating study. *Geochim. Cosmochim. Acta*, **70**, A303-A303.

**Keller W.D.** (1978) Classification of kaolin exemplified by their textures in scan electron micrographs. *Clays Clay Minerals,* **26,** 1-20.

**Keller, W. D., Reynolds, R.C.** and **Inoue, A.** (1986) Morphology of clay minerals in the smectite-to-illite conversion series by scanning electron microscopy. *Clays and Clay Minerals*, **34**, 187-197.

**Koren, I., Kaufman, Y.J., Washington, R., Todd, M.C., Rudich, Y., Martins, J.V.** and **Rosenfeld, D.** (2006) The Bodele depression: a single spot in the Sahara that provides of the mineral dust to the Amazon forest. Environ. Res. Lett., 1, 014005. https://doi.org/10.1088/1748-9326/1/1/014005.

**Kulke, H.** (1969) Petrographie und Diagenese des Stuben sandsteins (mittelerer Keuoer) aus Tief-bohrungen im Raum, Memmingen (Bayern). *Contributions to Mineralogy and Petrology.* **20**, 135-163

**Lidmar-Bergstrøm, K.** (1993) Denudation surfaces and tectonics in the southernmost part of the Baltic Shield. *Precambrian Research*, **64**, 337-345.

**Mahowald, N., Luo, C., del Corral, J.** and **Zender, C.S.** (2003) Interannual variability in atmospheric mineral aerosols from a 22-year model simulation and observational data. *J. Geophys. Res*., **108**, 1–20.

**Martin, J.E.** and **Parris, D.C. (**2007) The Geology and Paleontology of the Late Cretaceous Marine Deposits of the Dakotas. *Geological Society of America, GAS Special Paper*, **427**, doi.org/10.1130/SPE427.

**Matsuda, T**. and **Henmi, K.** (1983) Syntheses and properties of regularly interstratified 25Å minerals. *Clay Science,* **6**, 51-66.

**McKie, T.** and **Williams, B.P.J.** (2009) Triassic palaeogeography and fluvial dispersal across the northwest European Basins. *Geol. J.*, **44**, 711–741.

**Meyer, K.M., Yu, M., Jost, A.B., Kelley, B.M. and Payne, J.J.** (2011) δ13C evidence that high primary productivity delayed recovery from end-Permian mass extinction. *Earth and Planetary Science Letters*, **302**, 378-384.

**Monro, S. K., Loughnan, F. C.** and **Wallker, M. C**. (1983) The Ayrshire Bauxitic Clay: an allochthonous deposit? *In* Wilson, R. C. L. (ed.), *Residual deposits:surface related weathering processed and materials,* Geol. Soc. London, Spec. Publ. No. 11, Blackwell.

**Moore, D.M.** and **Reynolds, R.C. Jr.** (1997) *X-ray Diffraction and the Identification and Analysis of Clay Minerals.* Oxford University Press, New York.

**Morrison, S.** and **Parry, W.T.** (1986) Dioctahedral corrensite from Permian red beds, Lisbon Valley, Utah. *Clays and Clay Minerals,* **34**, 613-624.

**Morton, A. C.** (2012) Value of heavy minerals in sediments and sedimentary rocks for provenance, transport history and stratigraphic correlation, In: Sylvester, P. (ed.), Quantitative Mineralogy and Microanalysis of Sediments and Sedimentary Rocks: Mineralogical Association of Canada, Short Course Series, **42**, 133–165.

**Nadeau, P.H.** (2011) Earth's energy "Golden Zone": a synthesis from mineralogical research. *Clay Minerals*, **46**, 1–24.

**Nettleton, W.D.** and **Chadwick, O.A.** (1996) Late Quaternary, re-deposited loess-soil developmental sequences, South Yemen. *Geoderma*, 70, 21–36.

**Norling, E.** (1970) Jurassic and L. Cretaceous stratigraphy of the Rydeback—Fortuna borings in southern Sweden. *Geol. Feren. Forhand. Stockholm*, **92**, 261-87.

**Price, W. A.** (1963) Physicochemical and environmental factors in clay dune genesis. *Journal of Sedimentary Petrology*, **33,** 766-778.

**Reeves, G. M., Sims, I.** and **Cripps, J. C.** (2006) Clay Materials used in Construction. Geological Society, London, Engineering Geology Special Publication, **21**, 525 pp

**Reichow M.K., Pringle, M.S., Al'Mukhamedov, A.I., Allen, M.B., Andreichev, V.L., Buslov, M.M., Davies, C.E., Fedoseev, G.S., Fitton, J.G., Inger, S. , Medvedev, A.Ya., Mitchell, C., Puchkov, V.N., Safonova, I.Yu, Scott, R.A.** and **Saunders, A.D.** (2009). The timing and extent of the eruption of the Siberian Traps large igneous province: Implications for the end-Permian environmental crisis. *Earth and Planetary Science Letters*, **277**, 9–20.

**Retallack, G.J.** and **Krull, E.S.** (2006) Carbon isotopic evidence for terminal-Permian methane outbursts and their role in extinctions of animals, plants, coral reefs, and peat swamps. *In*: Greb, S.F., DiMichele, W.A. (eds.), Wetlands through time. *Geological Society of America*, Special Paper 399.

**Riber, L., Dypvik, H.** and **Sørlie, R**. (2015) Altered basement rocks on and around the Utsira High, Norwegian North Sea. *Nor. J. Geol.*, **95**, 57-89.

**Roscher, M., Stordal, F.** and **Svensen, H.** (2011) The effect of global warming and global cooling on the distribution of the latest Permian climate zones. *Palaeogeogr. Palaeoclimatol. Palaeoecol*., **309**, 186–200.

**Rust, B.R.** and **Nanson, G.C.** (1989) Bedload transport of mud as pedogenic aggregates in modern and ancient rivers. *Sedimentology*, **36**, 291-306.

**Sahney, S.** and **Benton, M.J.** (2008) Recovery from the most profound mass extinction of all time. *Proc. R. Soc. B.*, **275**, 759–765, doi:10.1098/rspb.2007.1370.

**Schoene, B., Eddy, M.P., Samperton, K>M>, Brenhin Keller, C., Keller, G., Adatte, T. and Khadri, S.F.R.** (2006) U-Pb constraints on pulsed eruption of the Deccan Traps across the end-Cretaceous mass extinction. *Science*, **363**, 862-866.

**Scoates, J.S.** and **Chamberlain, K.R.** (1995) Baddeleyite (ZrO2) and zircon (ZrSiO4) from anorthositic rocks of the Laramie anorthosite complex, Wyoming: petrologic consequences and U-Pb ages. *American Mineralogist*, **80**, 1317-1327.

**Shimoda, S.** (1969) New data for tosudite. *Clays and Clay Min.*, **17**, 179-184.

**Shimoda, S**. (1978) Interstratified minerals. *In:* Sudo, T. & Shimoda, S. (eds) *Clays and Clay Minerals of Japan.* Elsevier, Amsterdam, 265-322.

**Shumlyanskyy, L., Nosova, A., Billström, K., Söderlund, U., Andréasson, P-G**, and **Kuzmenkova, O.** (2016) The U-Pb zircon and baddelyite ages of the Neoproterozoic Volyn Large Igneous Province: implication for the age of the magmatism and the nature of a crustal contaminant. *GGF*, **138**, 17-30.

**Siivola, J.** (1977) Baddelyite - ZrO2 – from Lovasjärvi diabase, southeastern Finland. *Bulletin of the Geological Society of Finland*, **49**, 59-64.

**Singer, A.** (1984). The Palaeoclimatic interpretation of clay minerals in sediment - a review. *Earth Sci. Rev*., **21**, 251–293.

**Sun**, J, (2002) Provenance of loess material and formation of loess deposits on the Chinese Loess Plateau. *Earth and Planetary Science Letters*, **203**, 845-859.

**Sun, J, Ding, Z., Xia, X., Sun, M.** and **Windley, B.F.** (2018) Detrital zircon evidence for the ternary sources of the Chinese Loess Plateau. *Journal of Asian Earth Sciences*, **155**, 21-34.

**Soreghan, G. S.** (1992) Preservation and paleoclimatic significance of eolian dust in the Ancestral Rocky Mountains province. *Geology,* **20**, 1111-1114.

**Soreghan, G. S., Moses, A. M., Soreghan, M. J., Hamilton, M.A., Fanning, C. M.** and **Link, K.**, (2007) Palaeoclimatic inferences from upper Palaeozoic siltstone of the Earp Formation and equivalents, Arizona-New Mexico (USA). *Sedimentology,* **54**, 701-719.

**Soreghan, M.J., Soreghan, G.S.** and **Hamilton, M.A.** (2002) Palaeowinds inferred from detrital-zircon geochronology of upper Paleozoic loessite, western equatorial Pangea. *Geology,* **30**, 695–698.

**Soreghan, M.J., Heavens, N., Link, P.K., Hamilton, M.A.** and **Soreghan, G.S.** (2014) Abrupt and high-magnitude changes in atmospheric circulation recorded in the Permian Maroon Formation, tropical Pangea. *Geol. Soc. Am. Bull*., **126**, 569–584.

**Spears, D. A.** (2012) Origin of tonsteins, an overview and links with seatearths, fireclays and fragmental clay rocks. *International Journal of Coal Geology,* **94**, 22-31.

**Stevens, T., Carter, A., Watson, T.P., Vermeesch, P., Andò, D., Bird, A.F., Lu, H., Garzanti, E., Cottam, M.A.** and **Sevastjanova, I.** (2013) Genetic linkage between the Yellow River, the Mu Us desert and the Chinese Loess Plateau. *Quaternary Science Reviews*, **78**, 355-368.

**Sturt, B.A., Dalland, A.** and **Mitchell, J.L.** (1979) The age of the sub Mid-Jurassic weathering profile of Andøy, N. Norway, and the implications of the late Palaeozoic palaeogeography in the North Atlantic region. *Geol. Rundschau,* **68**, 523-542.

**Surdam, R.C., Crossey, L.J., Hagen, E.S.** and **Heasler, H.P.** (1989) Organic-inorganic interactions and sandstone diagenesis. American Association of Petroleum Geologists Bulletin, **73**, 1–23.

**Svensen, H., Planke, S., Malthe-Sorenssen, A., Jamtveit, B., Myklebust, R., Rasmussen Eidem, T., et al.,** (2004) Release of methane from a volcanic basin as a mechanism for initial Eocene global warming. *Nature*, **429**, 542–545.

**Svensen, H., Planke, S., Polozov, A.G., Schmidbauer, N., Corfu, F., Podladchikov, Y.Y.** and **Jamtveit, B.** (2009) Siberian gas venting and the end-Permian environmental crisis. *Earth Planetary Sciecne Letters*, **227**, 490-500.

**Talbot, M.R., Holm, K.** and **Williams, M.A.J.** (1994) Sedimentation in low-gradient desert margin systems: A comparison of the Late Triassic of northwest Somerset (England) and the late Quaternary of east-central Australia. *In:* Rosen, M.R. (ed) *Paleoclimate and basin evolution of Playa Systems*. Geological Society of America, Special Papers**, 289**, 97-117.

**Tan, P., Oberhardt, N., Dypvik, H., Riber, L.** and **Ferrell Jr, R.** (2017) Weathering profiles and clay mineralogical developments, Bornholm, Denmark. *Marine and Petroleum Geology*, **80**, 32-48.

**Taylor, K.G.** and **Macquaker, J.H.S.** (2014) Diagenetic alterations in a silt- and clay-rich mudstone succession: an example from the Upper Cretaceous Mancos Shale of Utah, USA. *Clay Minerals*, **49**, 213-227.

**Vandenberghe, J.** (2013) Grain size of fine-grained windblown sediment: a powerful proxy for process identification. *Earth Science Reviews*, **121**, 18-30.

**Wang, X., Lang, L., Li, H., Hua, T., Wang, G., Zhouo, N.** and **Jial, L.** (2015) Geochemical evidence for seasonal variations in potential loess sources of the western Chinese Loess Plateau. *Atmospheric Environment*, **120**, 369-375.

**Welton, J.** (1984) SEM Petrology Atlas. AAPG Methods in Exploration, AAPG vol. 4, DOI: https://doi.org/10.1306/Mth4442 ISBN electronic: 9781629811611

**Wignall, P.** (2005) The link between large igneous eruptions and mass extinctions. *Elements*, **1**, 293-297.

**Wilkins, A. D., Wilson, M. J., Morton, A. C., Hurst, A.** and **Archer, S. G.** (2015) First recorded occurrence of detrital badelleyite ($ZrO_2$) in sedimentary rock, (Smith Bank Formation, Triassic, Central North Sea). *Scottish Journal of Geology*. **51**, 185-189.

**Wilkins, A. D.** (2016) *Characterization of Triassic mudstones from the Central North Sea: sedimentological, mineralogical and pore system properties.* Unpublished PhD thesis, University of Aberdeen, 412pp

**Wilkins, A. D., Hurst, A, Wilson, M. J.** and **Archer, S.** (2017) Palaeoenvironment in an ancient low-latitude, arid lacustrine basin with loessite: the Smith Bank Formation (early Triassic) in the Central North Sea Continental Shelf. *Sedimentaology*, in press.

**Wilson, M. J.** (1971) Clay mineralogy of the Old Red Sandstone (Devonian) of Scotland. *Journal of Sedimentary Petrology*. **41**, 995-1007.

**Wilson, M. J.** (2013) *Sheet Silicates: Clay Minerals.* (Rock-Forming Minerals: Deer, Howie and Zussman). **3C**. Geological Society, London.

**Won, C., Hing, H., Cheng, F., Fang, Q., Wang, C., Zhao. L.** and **Churchman, G.J.** (2018) Clay mineralogy and its palaeoclimatic significance in the Luochuan loess-palaeosols over ~1.3 Ma, Shaanxi, northwestern China. *Front. Earth Sci*., **12**, 134-147.

**Wright, V.P.** and **Marriot, S.B.** (2007) The dangers of taking mud for granted: lessons from Lower Old Red Sandstone dryland river systems of South Wales. *Sedimentary Geology*, **195**, 91-100.

**Yaalon, D.H.** (1987) Saharan dust and desert loess: effect on surrounding soils. *Journal of African Earth Science*, **6**, 569-571.

**Zhao, L., Ward, C.R., French, D.** and **Graham, I. T.** (2015) Major and trace element geochemistry of coals and intra-seam claystones from the Songzao Coalfield, SW China. *Minerals,* **5**, 870-893.

**Ziegler, K.** (2006) Clay minerals of the Permian Rotliegend Group in the North Sea and adjacent areas. *Clay Minerals,* **21**, 355-393.

## FIGURE CAPTIONS

**Fig. 1.** (A) Location of well 20/25-1 in the UK Central North Sea with an outline of the possible lacustrine area coeval with loessite deposition. (B) Location of samples and the sedimentary log of the cored interval (after Wilkins et al., 2017).

**Fig. 2.** X-ray diffraction (XRD) traces of the clay fractions from well 20/25-1: (A) sample SB01, planar grain fabric; (B) sample SB07, planar grain fabric; (C) sample SB05, random grain fabric. Air-dried (black), ethylene glycol treated (blue) and heated at 300ºC (red). Tos = tosudite, Ch = chlorite, K = kaolinite, I = illite, I/S = mixed-layer illite/smectite. All samples using Co Kα radiation.

**Fig. 3.** X-ray diffraction (XRD) traces of the clay fraction of SB01 to demonstrate the identification of tosudite following air-drying (black), ethylene glycol (blue) heating at 300°C (red) and HCl treatment (green). Note the persistence of the high spacing peak after HCl treatment. Tos = tosudite, I = illite, I/S = mixed-layer illite/smectite, and K = kaolinite.

**Fig. 4.** Back-scattered scanning electron microscopy (BSEM) images: (A) unstratified loessite with random fabric as seen by the disposition of muscovite and biotite flakes; (B) stratified loessite with planar fabric emphasized by the common orientation of muscovite flakes; (C) fabric showing entire or partly disaggregated clay pellets; (D) kaolinitized biotite mica; (E) intercalated kaolinite in exfoliated mica; (F) occurrence of chlorite (c) as thin dark layers, intercalated within muscovite.

**Fig. 5.** Energy dispersive spectroscopy (EDS) spectra showing the compositions of: (A) chlorite with Mg-rich composition; (B) biotite mica with peaks for K, Fe and Mg.

**Fig. 6.** Back-scattered scanning electron microscopy (BSEM) images of quartz: (A) irregular, embayed (elongate grain with fluid inclusions) and ragged margins (middle and lower left) and trails of fluid inclusions (arrows); (B) jigsaw contacts (j) indicative of micro-fractures formed by mechanical breakage during compaction.

**Fig. 7.** Scanning electron microscopy (SEM) images of a rock fragment showing tosudite occurring as: (A) a pseudo-honeycomb fabric similar to that of dried down smectitic clays; (B) a coating of tosudite on a hexagonal kaolinite crystal. (C) Energy dispersive spectroscopy (EDS) spectrum of tosudite in (A) showing a strong Al peak and a significant Mg peak.

**Fig. 8.** Scanning electron microscopy (SEM) images of rock fragments showing: (A) euhedral pyramidal crystals of quartz (**q**) growing through a matrix of tosudite (**t**), rhombohedral diagenetic crystal of dolomite (**d**) and irregular book-like stack of kaolinite (**k**); (B) diagenetic quartz penetrating pseudo-honeycomb fabric of tosudite; (C) a vermicular aggregate of kaolinite within which a 5 µm diameter pore (p) occurs.

**Fig. 9.** Scanning electron microscopy (SEM) images and selected energy dispersive spectroscopy (EDS) spectra from rock fragments: (A) euhedral crystals of apatite and K-feldspar; (B) EDS spectrum of apatite showing strong Ca and P peaks; (C) euhedral diagenetic albite; (D) EDS spectrum of albite crystal showing peaks for Si, Al and Na; (E) euhedral halite crystals (**h**) in a matrix of small kaolinite aggregates; (F) EDS spectrum of halite showing strong Na and Cl peaks.

**Fig. 10.** Back-scattered scanning electron microscopy (BSEM) of thin sections: (A) two examples of well-shaped baddeleyite crystals ($ZrO_2$), dark holes in the baddeleyite are caused by the energy dispersive spectroscopy (EDS) beam (after Wilkins et al., 2015, scale bar is 4 µm); (B) a silt-sized grain with micron-scale, bright (high electron density) Ti mineralization, highly irregular geometry quartz grains (in the lower part of the image) and twisted mica flakes (upper centre of image).

**Fig. 11.** Mineral provenance depicted in three source-terrane domains, sedimentary, basic magmatic and acid–intermediate magmatic demonstrating individual minerals that are important diagnostically and often typical only of a specific terrane (bold) with other non-terrane-specific minerals. Apt = apatite, **Bdlt** = baddeleyite, Biot = biotite, Chlt = chorite, Illt

= illite, Kaol – kaolinite, Ksp = K-feldspar, Musc = muscovite, **Plag** = plagioclase feldspar, Qtz = quartz, **Qtz2** = quartz with irregular geometry, **San** = sanidine feldspar, **Tos** = tosudite, Zrc = zircon. Information is relevant to the Smith Bank Formation (SBF) in this study and may not have global relevance.

**Fig. 12.** Grain size and textural charactersitics of different forms of kaolinite in scanning electron microscopy (SEM) images: (A) an irregular book-like stack of kaolinite intercalated with quartz (q); (B) vermicular kaolinite with a large (*ca* 5 μm) open pore space; (C) matrix of small irregular kaolinite aggregates. The same scale applies to all images.

**Fig. 13.** (A) Palaeo-geography during the Early Triassic showing the location of the study area (ellipse), prevailing winds, a possible southerly air flow near the confluence of the Polar High Pressure and Westerlies (open arrow), and location of the Siberian Traps (ST). (B) Reconstruction of the lacustrine area of the North Permian Basin during the Early Triassic showing the location of well 20/25-1, the likely direction of aerosol dust input to the basin, the prevailing south-easterly winds recorded in aeolian dunes. A hypothetical location of pre-Triassic kaolinitic regolith (dotted area) that extended eastward at least into southern Sweden and the western area of the present-day Baltic Sea.

| | Depth (m) | Quartz | Plagioclase | K'spar | Dolomite | Halite | Hematite | Illite | Kaolinite | Tosudite | Chlorite |
|---|---|---|---|---|---|---|---|---|---|---|---|
| SB01 | 1649.7 | 46.9 | 7.2 | 6.5 | 1.8 | 1.5 | 2.3 | 20.2 | 4.0 | 6.8 | 2.5 |
| SB02 | 1650.9 | 44.1 | 7.0 | 6.0 | 11.6 | 0.9 | 1.9 | 17.2 | 3.9 | 4.7 | 2.4 |
| SB03 | 1654.5 | 35.7 | 7.4 | 5.8 | 8.9 | 0.5 | 2.6 | 25.9 | 2.6 | 7.0 | 3.3 |
| SB04 | 1656.7 | 39.5 | 7.3 | 5.8 | 11.8 | 0.5 | 1.8 | 23.1 | 1.6 | 5.1 | 3.2 |
| SB05 | 1657.4 | 34.9 | 7.0 | 5.9 | 7.8 | 0.5 | 2.5 | 27.6 | 3.4 | 7.7 | 2.4 |
| SB06 | 1660.8 | 38.7 | 6.8 | 6.2 | 7.4 | 0.4 | 0.4 | 27.4 | 3.0 | 6.9 | 2.5 |
| SB07 | 1663.0 | 35.6 | 5.4 | 5.8 | 3.0 | 1.1 | 2.6 | 30.8 | 3.6 | 8.4 | 3.3 |
| SB08 | 1652.5 | 41.7 | 7.5 | 5.2 | 9.8 | 0.5 | 1.6 | 23.5 | 3.6 | 0.0 | 6.6 |
| SB09 | 1661.8 | 42.7 | 7.1 | 6.4 | 3.8 | 0.6 | 1.3 | 26.5 | 3.3 | 3.0 | 5.4 |
| SB10 | 1662.8 | 35.6 | 6.0 | 5.0 | 29.5 | 0.4 | 0.3 | 15.2 | 2.9 | 0.0 | 5.0 |

**Table 1.** Bulk analyses of mineralogy samples from well 20/25-1 determined by XRD; K'spar = potassium feldspars.

| | Depth (m) | Illite | Kaolinite | Tosudite | Chlorite | I/S |
|---|---|---|---|---|---|---|
| SB01 | 1649.7 | 37 | 21 | 21 | 13 | 8 |
| SB02 | 1650.9 | 28 | 22 | 16 | 11 | 23 |
| SB03 | 1654.5 | 44 | 17 | 10 | 15 | 16 |
| SB04 | 1656.7 | 48 | 9 | 12 | 13 | 18 |
| SB05 | 1657.4 | 43 | 14 | 12 | 15 | 17 |
| SB06 | 1660.8 | 43 | 12 | 12 | 13 | 20 |
| SB07 | 1663.0 | 44 | 19 | 10 | 16 | 11 |
| SB08 | 1652.5 | 36 | 17 | 14 | 13 | 21 |
| SB09 | 1661.8 | 38 | 20 | 10 | 15 | 18 |
| SB10 | 1662.8 | 32 | 23 | 13 | 18 | 14 |

**Table 2.** Clay mineralogy of clay fractions (<2.0 μm) in samples from well 20/25-1. I/S = mixed layer illite/smectite.

| | | | |
|---|---|---|---|
| **Quartz** | Angular silt | Irregular geometry | |
| **Illite/mica** | Clay-sized illite | Randomly oriented muscovite | Euhedral biotite |
| **Feldspar**<br>**Plagioclase (p)**<br>**Orthoclase (k)** | Angular silt | P > K | |
| **Tosudite** | Amorphous groundmass | Diagenetic crystals in pores | |
| **Baddeleyite** | Tiny euhedral grains | | |
| **Shards** | Silt sized | Ti mineralized | |
| | | | |
| **Clay pellets** | Coarse silt-sized particles | | |
| **Kaolinite** | Vermicules in clay pellets | Coarse silt-sized booklets | |

**Table 3.** Mineralogical and petrographic characteristics relevant to the differentiation of aerosol dust source terrane. Light grey background indicates likely long distance sourcing. Darker grey background indicates local sourcing.

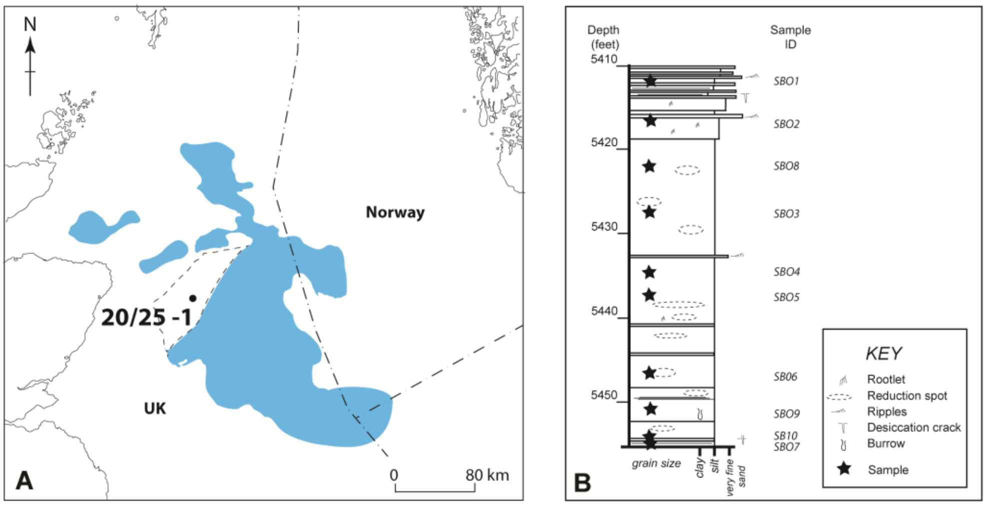
N
Norway
20/25 -1
UK
0
80 km
A
Depth
(feet)
Sample
ID
5410
5420
5430
5440
5450
SBO1
SBO2
SBO8
SBO3
SBO4
SBO5
SB06
SBO9
SB10
SBO7
grain size
clay
silt
very fine sand
KEY
Rootlet
Reduction spot
Ripples
Desiccation crack
Burrow
Sample
B

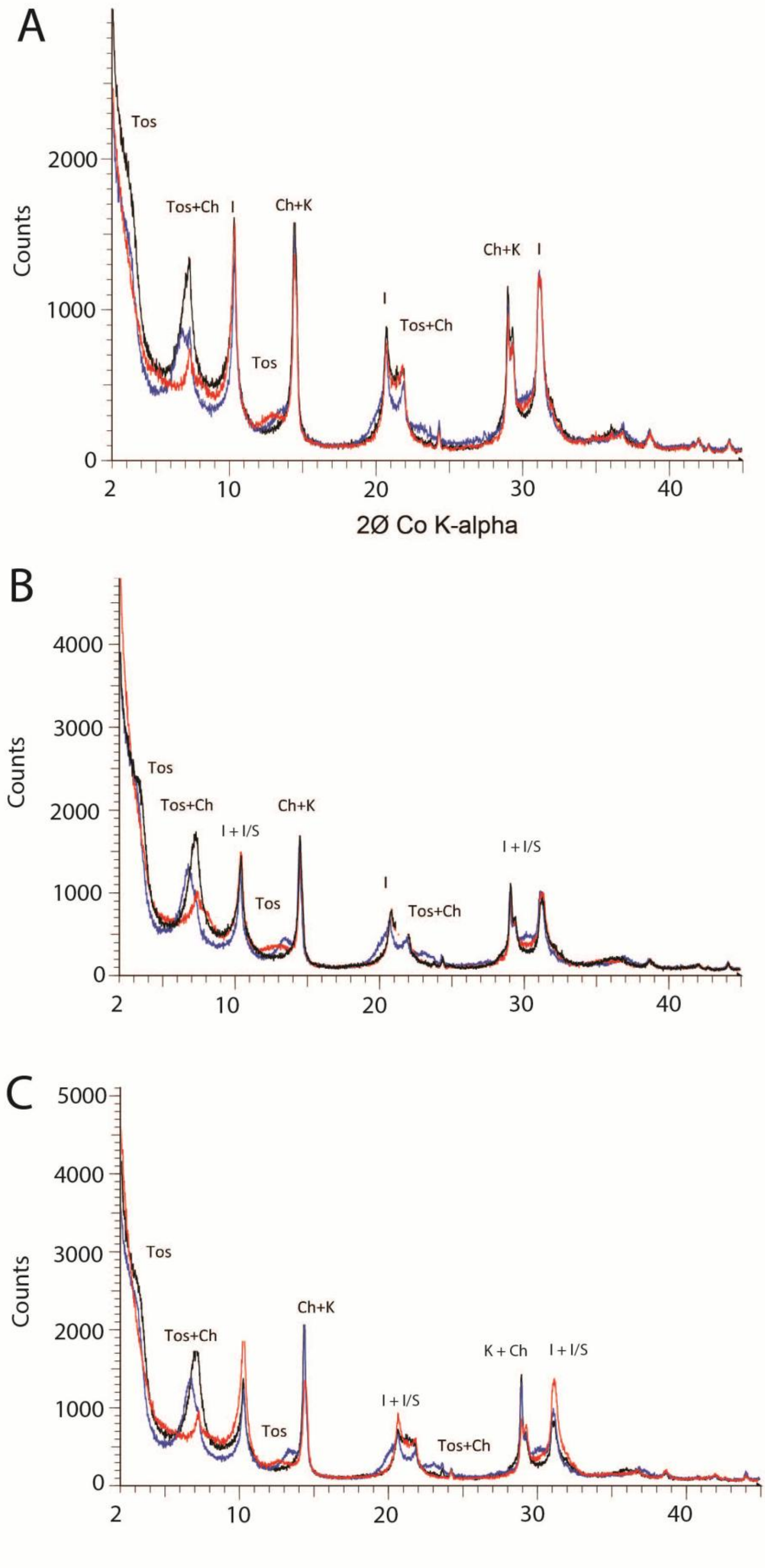

A
Counts
Tos
Tos+Ch
I
Ch+K
Tos
I
Tos+Ch
Ch+K
I
2Ø Co K-alpha
B
Counts
Tos
Tos+Ch
I + I/S
Ch+K
Tos
I
Tos+Ch
I + I/S
C
Counts
Tos
Tos+Ch
Ch+K
Tos
I + I/S
Tos+Ch
K + Ch
I + I/S

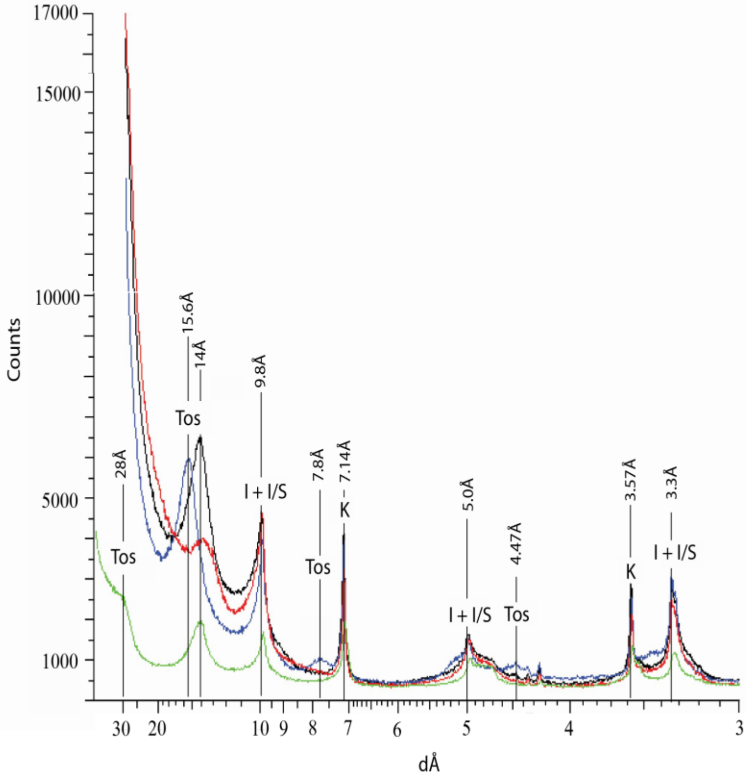

17000
15000
10000
5000
1000
Counts
28Å
Tos
15.6Å
14Å
Tos
9.8Å
I + I/S
7.8Å
Tos
K - 7.14Å
5.0Å
I + I/S
4.47Å
Tos
3.57Å
K
3.3Å
I + I/S
30 20 10 9 8 7 6 5 4 3
dÅ

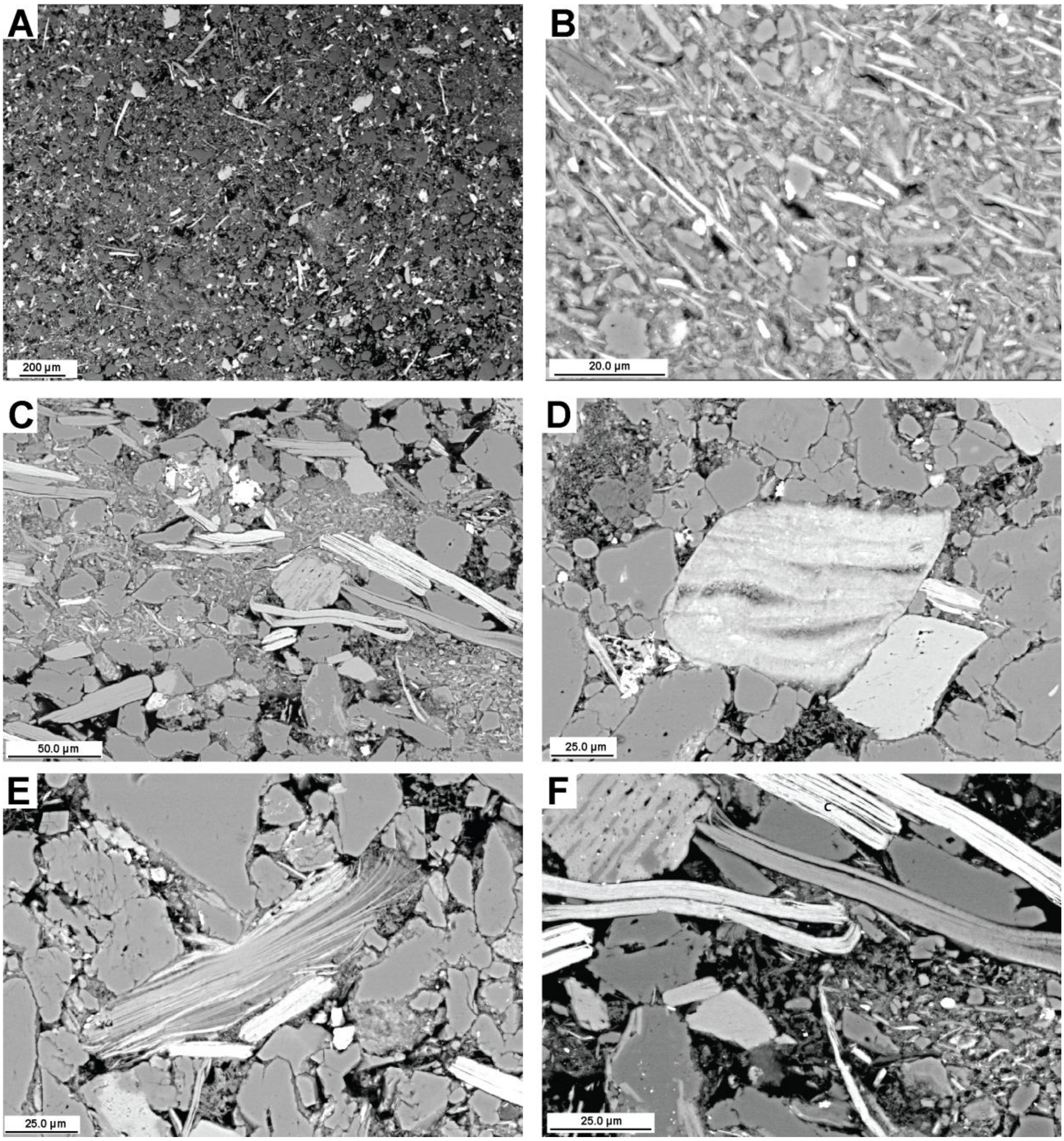
A
200 µm
B
20.0 µm
C
50.0 µm
D
25.0 µm
E
25.0 µm
F
25.0 µm

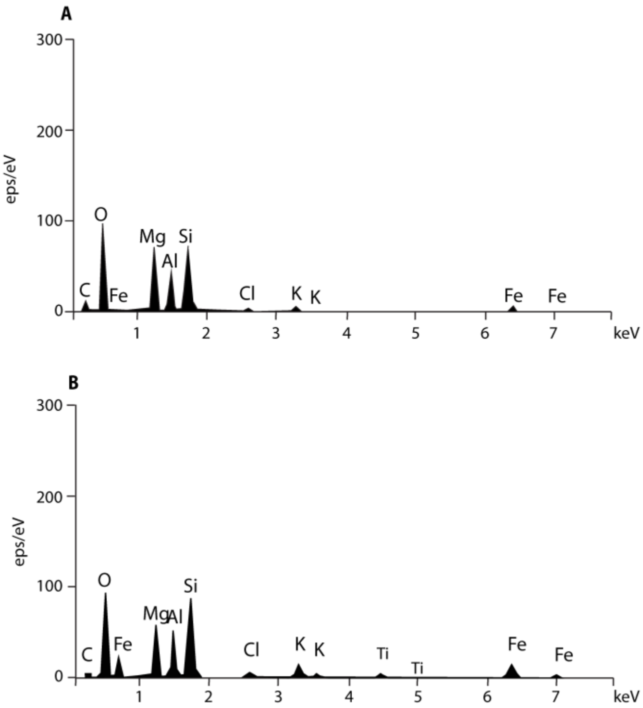
A
B
300
200
100
0
eps/eV
O
Mg
Si
Al
C
Fe
Cl
K
Ti
1
2
3
4
5
6
7
keV

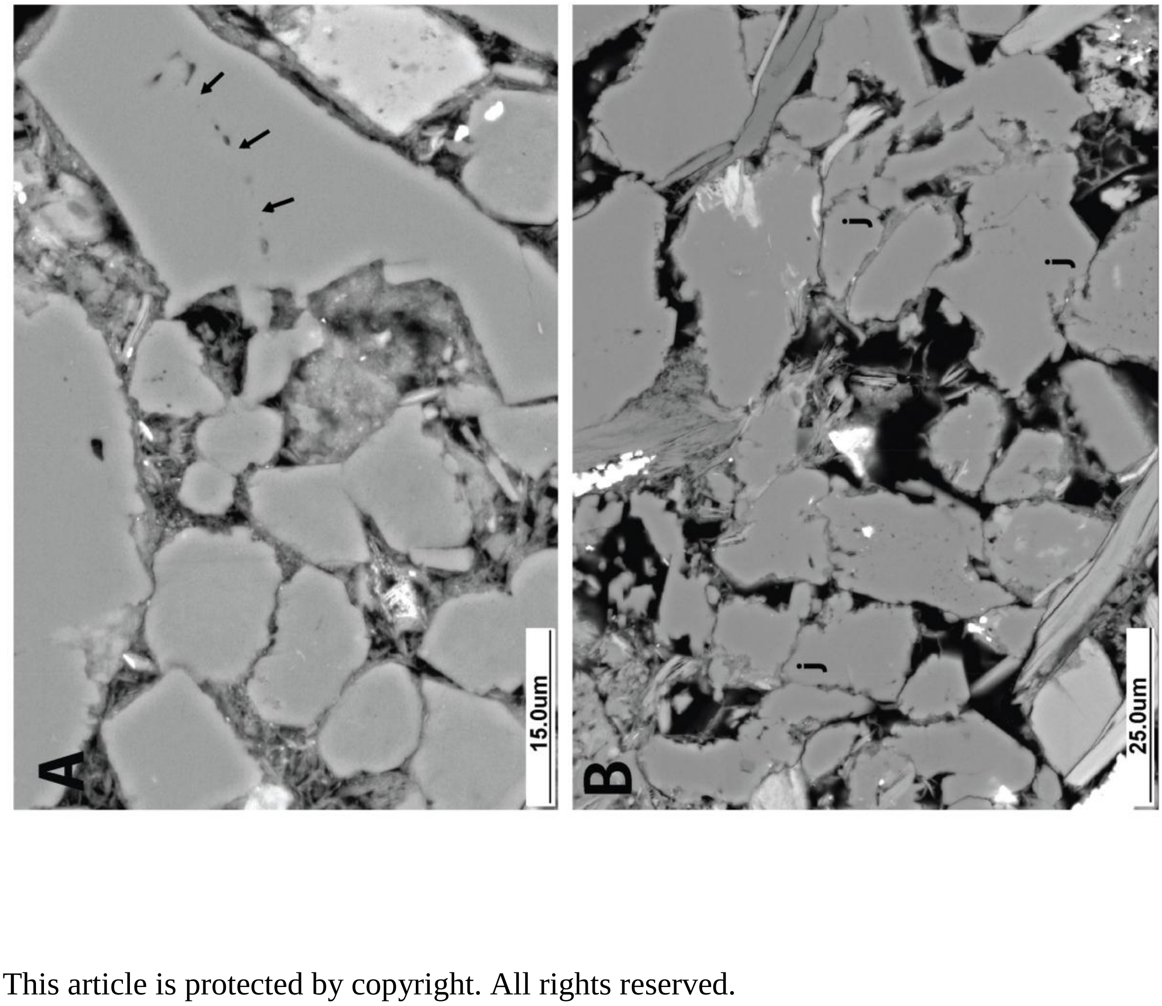
A
15.0um
B
25.0um

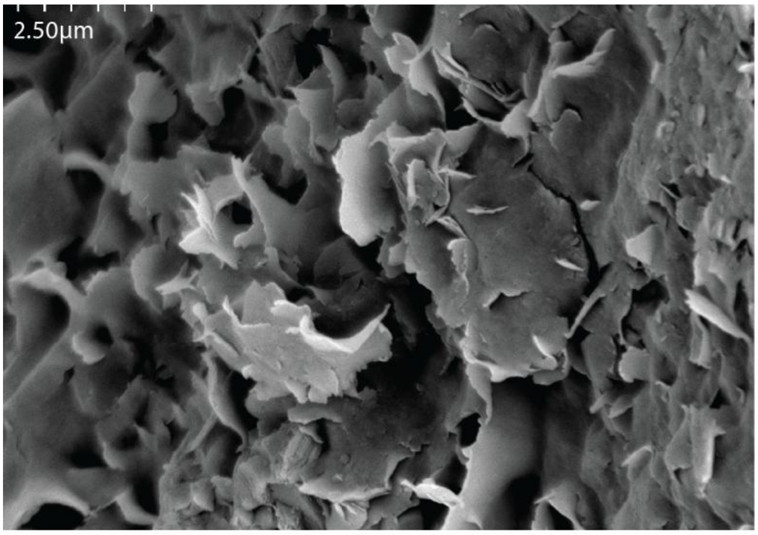
2.50µm

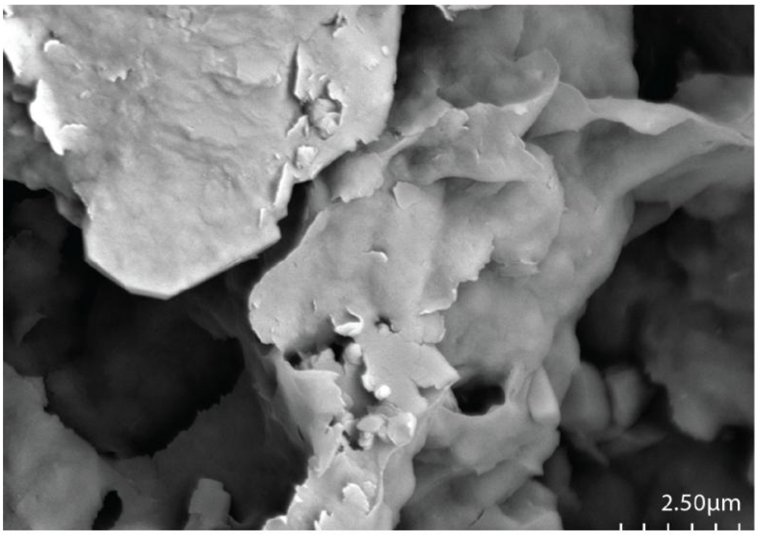
2.50µm

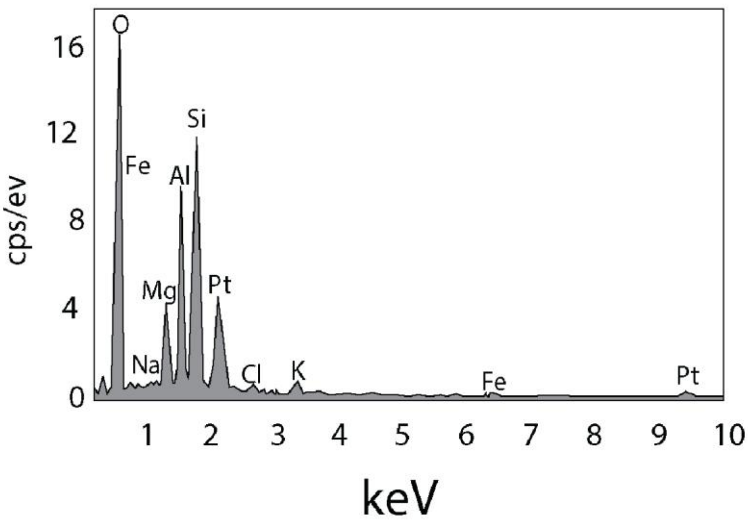
O
Si
Fe
Al
Mg
Pt
Na
Cl
K
Fe
Pt
cps/ev
0
4
8
12
16
1
2
3
4
5
6
7
8
9
10
keV

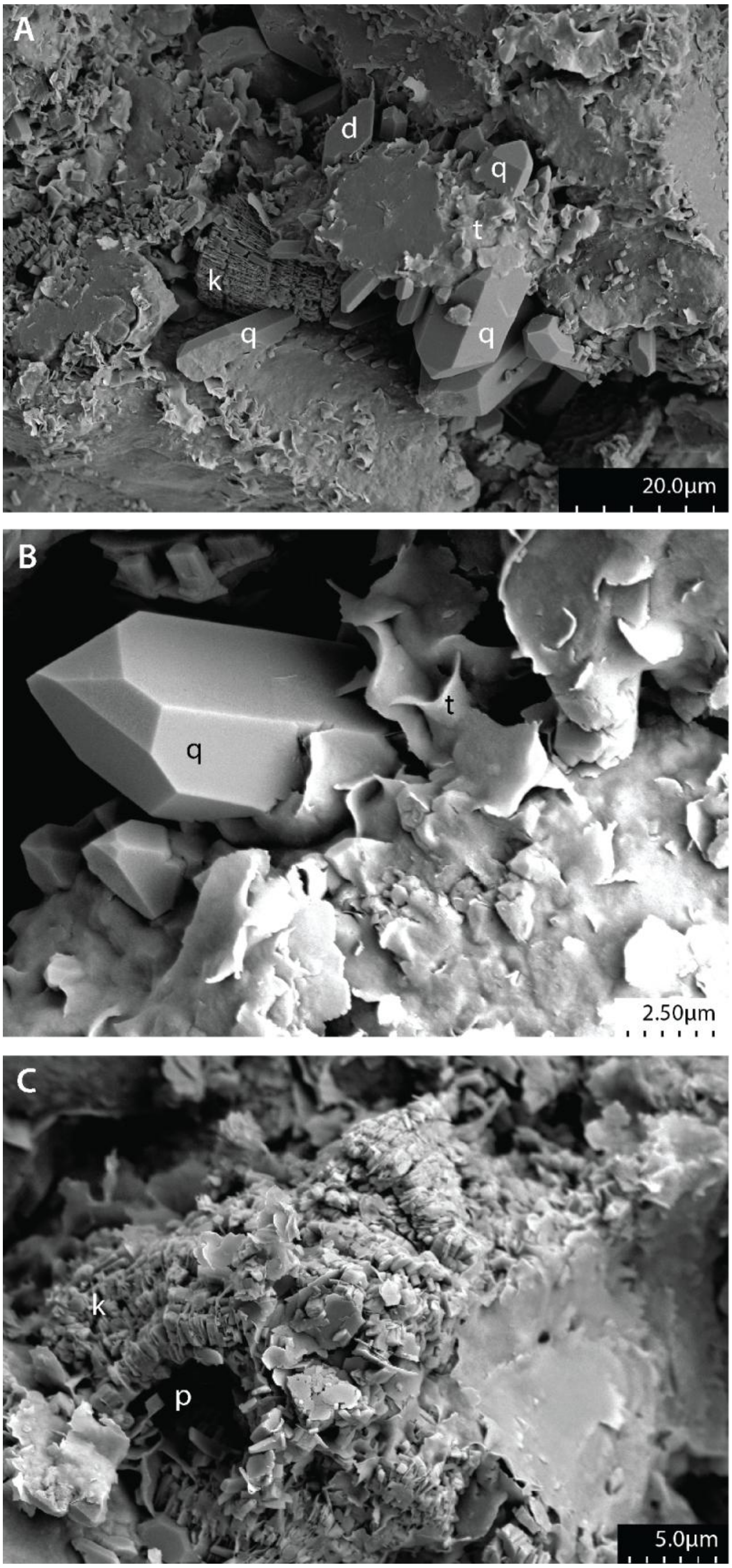
A
d
q
t
k
q
q
20.0µm
B
q
t
2.50µm
C
k
p
5.0µm

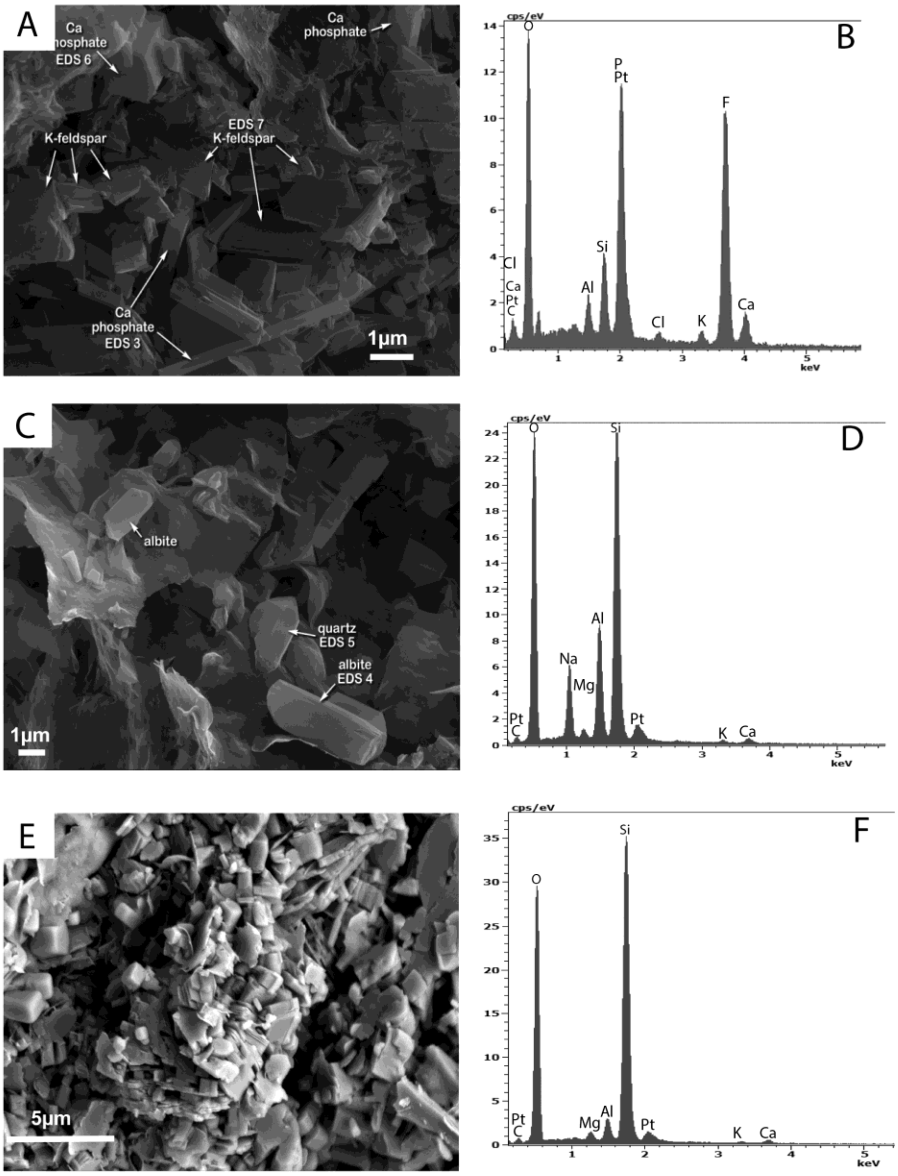
A
Ca phosphate EDS 6
Ca phosphate
K-feldspar
EDS 7 K-feldspar
Ca phosphate EDS 3
1µm
B
cps/eV
O
P Pt
F
Si
Cl
Ca Pt C
Al
Cl
K
Ca
keV
C
albite
quartz EDS 5
albite EDS 4
1µm
D
cps/eV
O
Si
Al
Na
Mg
Pt C
Pt
K
Ca
keV
E
5µm
F
cps/eV
Si
O
Pt C
Mg
Al
Pt
K
Ca
keV

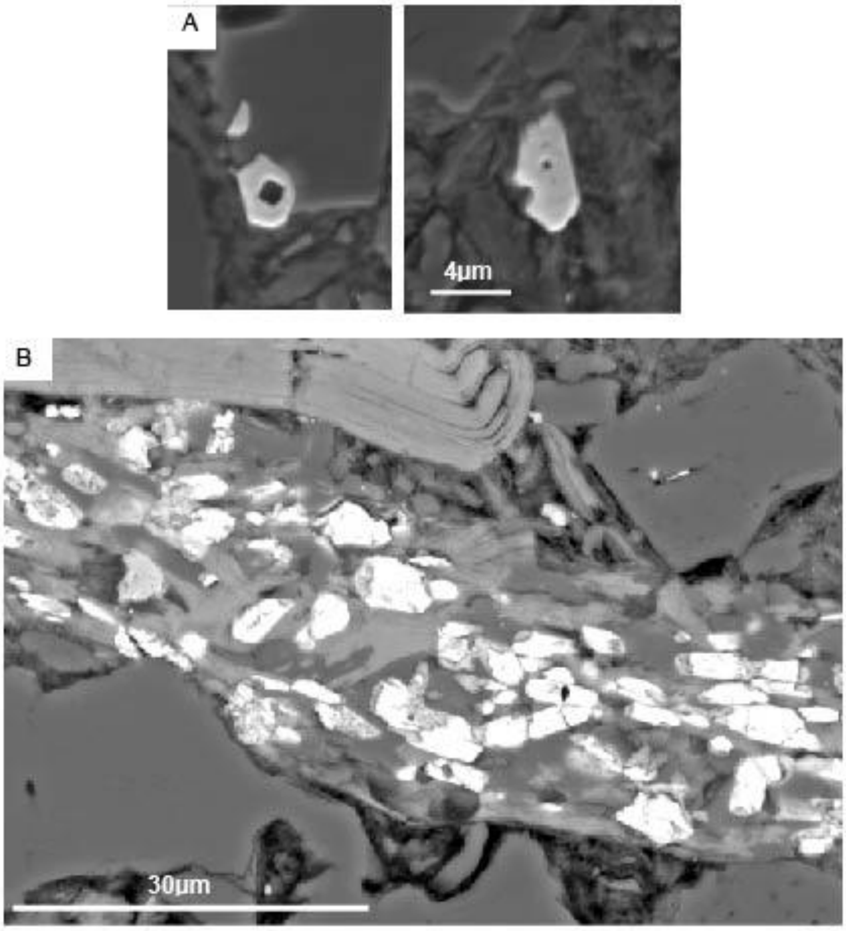
A
4µm
B
30µm

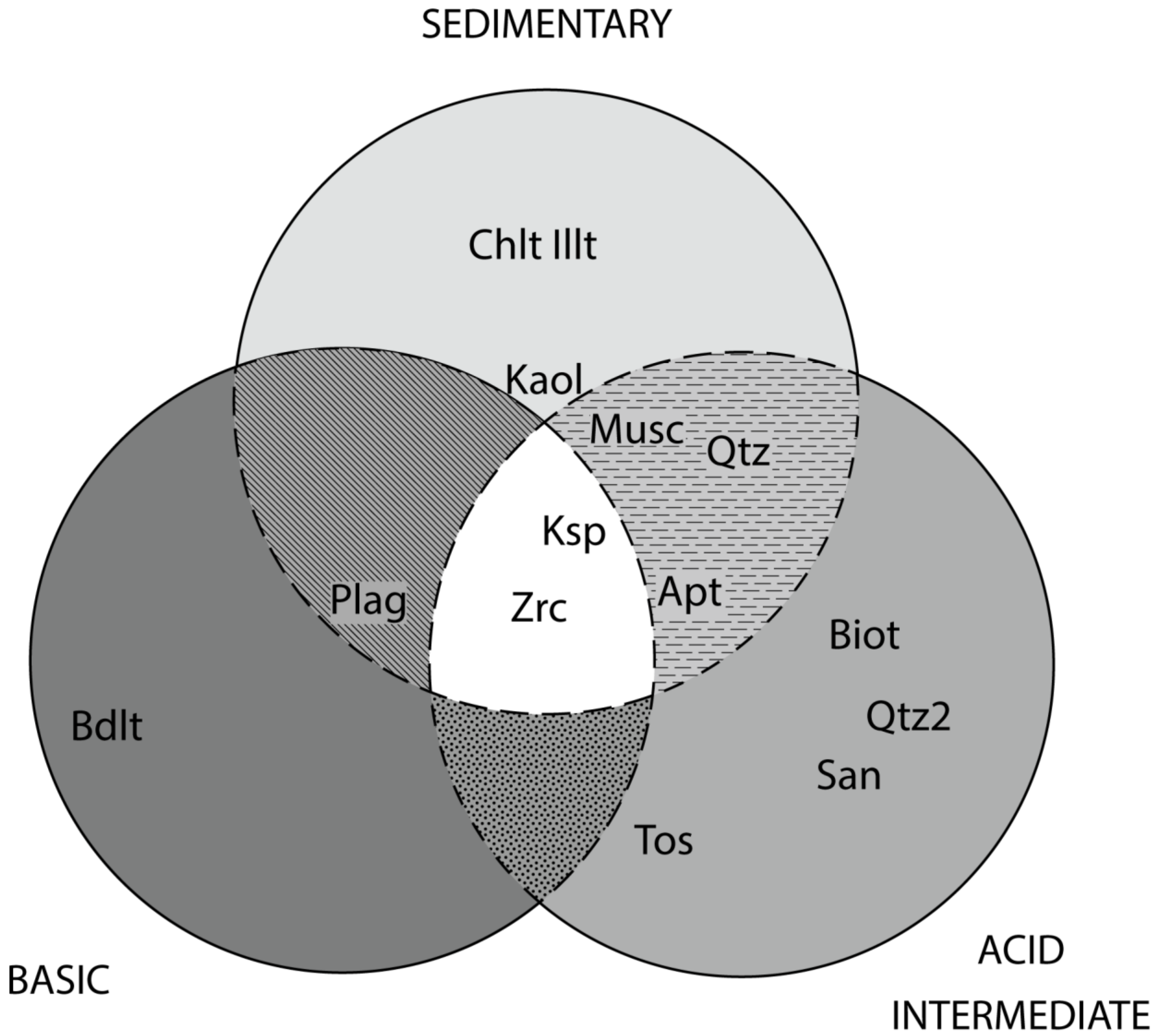
SEDIMENTARY
Chlt Illt
Kaol
Musc
Qtz
Ksp
Zrc
Plag
Apt
Biot
Bdlt
Qtz2
San
Tos
BASIC
ACID
INTERMEDIATE

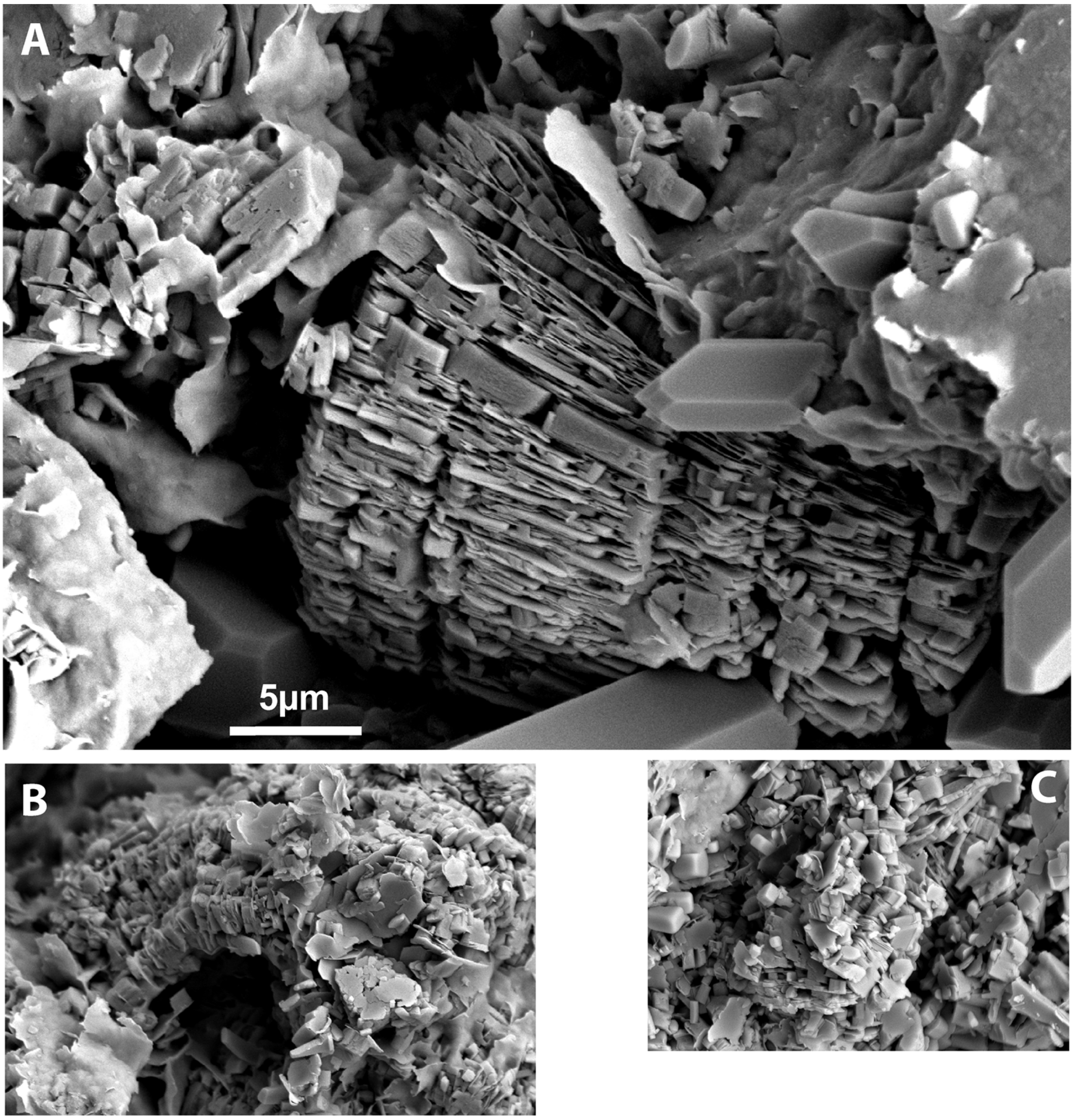
A
5µm
B
C

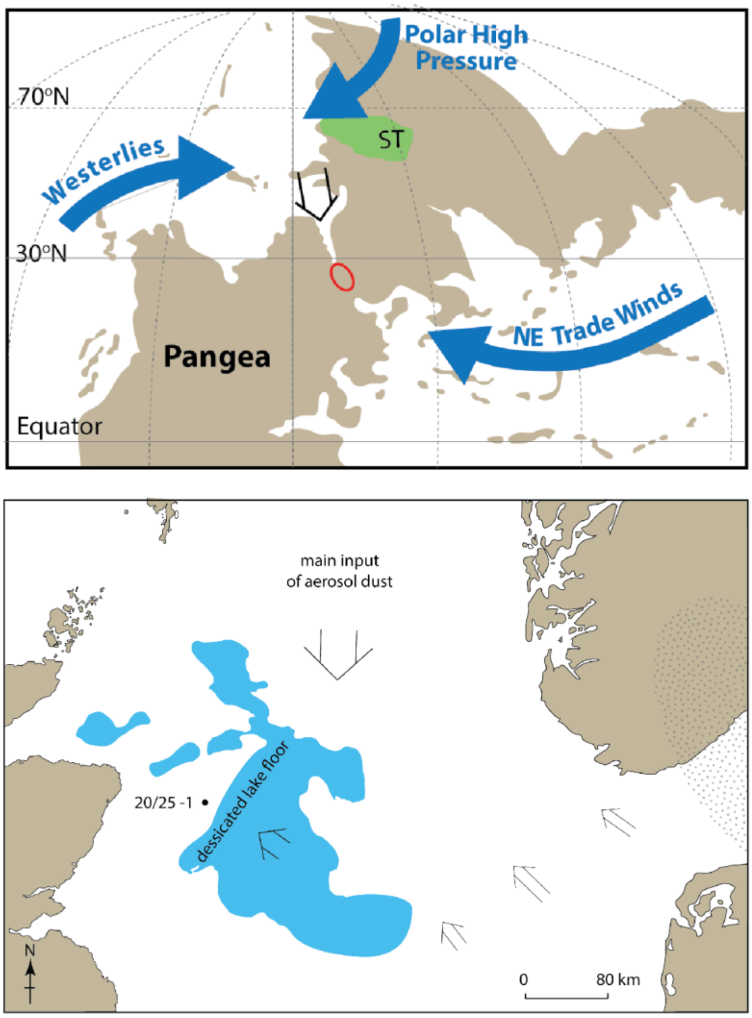
Polar High
Pressure
70°N
ST
Westerlies
30°N
Pangea
NE Trade Winds
Equator
main input
of aerosol dust
20/25 -1
dessicated lake floor
N
0
80 km